BARC/2019/E/002

BARC/2019/E/002

भारत सरकार
Government of India

BARC REPORT

EXTERNAL

BEHAVIOR OF A SOIL COLUMN SUBJECTED TO HARMONIC EXCITATION FOR LOW AND HIGH STRAINS

by

Raj Banerjee, Srijit Bandyopadhyay, G.R. Reddy and Tarvinder Singh

Structural and Seismic Engineering Section

Justin Coleman and Chandrakanth Bolisetti

Facility Risk Group

Idaho National Laboratory, Idaho Falls

भाभा परमाणु अनुसंधान केंद्र
Bhabha Atomic Research Centre
मुंबई Mumbai - 400 085, भारत India

2019

BARC/2019/E/002

BARC/2019/E/002

GOVERNMENT OF INDIA
DEPARTMENT OF ATOMIC ENERGY

BEHAVIOR OF A SOIL COLUMN SUBJECTED TO HARMONIC EXCITATION FOR LOW AND HIGH STRAINS

by

Raj Banerjee*, Srijit Bandyopadhyay,
G.R. Reddy and Tarvinder Singh
rbanerjee@barc.gov.in*
Structural and Seismic Engineering Section

Justin Coleman and Chandrakanth Bolisetti
Facility Risk Group
Idaho National Laboratory, Idaho Falls

BHABHA ATOMIC RESEARCH CENTRE
MUMBAI, INDIA
2019

BIBLIOGRAPHIC DESCRIPTION SHEET FOR TECHNICAL REPORT
(as per IS : 9400 - 1980)

01	*Security classification :*	Unclassified
02	*Distribution :*	External
03	*Report status :*	New
04	*Series :*	BARC External
05	*Report type :*	Technical Report
06	*Report No. :*	BARC/2019/E/002
07	*Part No. or Volume No. :*	
08	*Contract No. :*	
10	*Title and subtitle :*	Behavior of a soil column subjected to harmonic excitation for low and high strains
11	*Collation :*	62 p., 41 figs., 3 tabs.
13	*Project No. :*	
20	*Personal author(s) :*	1.Raj Banerjee, Srijit Bandyopadhyay, G.R. Reddy, Tarvinder Singh 2. Justin Coleman
21	*Affiliation of author(s) :*	1. Structural and Seismic Engineering Section, Bhabha Atomic Research Centre, Mumbai 2. Facility Risk Group, Idaho National Laboratory, USA
22	Corporate author(s):	Bhabha Atomic Research Centre, Mumbai - 400 085
23	*Originating unit :*	Structural and Seismic Engineering Section, Bhabha Atomic Research Centre, Mumbai
24	*Sponsor(s) Name :* *Type :*	Department of Atomic Energy Government

Contd...

30	*Date of submission :*	May 2019
31	*Publication/Issue date :*	May 2019
40	*Publisher/Distributor :*	Head, Scientific Information Resource Division, Bhabha Atomic Research Centre, Mumbai
42	*Form of distribution :*	Hard copy
50	*Language of text :*	English
51	*Language of summary :*	English
52	*No. of references :*	37 refs.
53	*Gives data on :*	

60 *Abstract :* Design Basis Ground Motion is generally defined on rock outcrop because, in general safety related nuclear structures are founded on rock. For sites at which the bedrock is very deep, these safety related structures are founded on soil. Consequently, the behaviour of the foundation of structures resting on soil is very much different than on bedrock. Hence, seismic ground response analysis is required to develop a site-specific response spectrum for the design of important superstructures in the region. One-dimensional ground response analysis is a commonly used method to estimate the ground responses under earthquake excitation in both equivalent linear and non-linear domains for both low to high strains. To understand the above phenomena, tests on F-55 Ottawa sand have been performed in a large scale geotechnical laminar box (GLB) at the Buffalo State University, New York. In this study, these tests have been simulated using numerical procedures involving equivalent linear and nonlinear time history analysis (using hyperbolic stress strain curve) using the author's in-house code which is limited to low to medium strains. The developed code, when tested for high strains, results in response accelerations that are lower than the experimental observations. The limitation of the model is that it predicts higher damping under larger strains. To match the damping under large strains, a modification is introduced in the developed nonlinear model which takes into account the above problem. With this modification, the predicted accelerations are in line with the experimental observation. Further, a study illustrating the performance of hyperbolic and multilinear backbone curves are studied based on the generation of the amplitude of high frequency harmonics in the response of nonlinear soil at high degree of nonlinearity. It is observed that the amplitude of odd harmonics is dependent on the number of parallel springs (or number of points) chosen for generating the multilinear stress strain curve and it is least (minimum) if a continuous (hyperbolic) backbone curve is chosen for conducting the nonlinear analysis of soil column. In addition, the results of the dynamic model tests are compared with the results from a plane strain finite difference program in terms of acceleration time history at the top and bottom accelerometer locations and it is found out that the numerical predictions are in reasonable agreement with the experimental observation using hyperbolic nonlinear stress-strain soil model

70 *Keywords/Descriptors :* REACTOR DESIGN; REACTOR SAFETY; NUCLEAR FACILITIES; STRESSES; SOIL-STRUCTURE INTERACTIONS; SITE SELECTION; SEISMIC EFFECTS; STRAIN RATE

71	*INIS Subject Category.:*	S22
99	*Supplementary elements :*	

BEHAVIOR OF A SOIL COLUMN SUBJECTED TO HARMONIC EXCITATION FOR LOW AND HIGH STRAINS

Raj Banerjee[1]*, Srijit Bandyopadhyay[1], G.R. Reddy[1], Tarvinder Singh[1], Justin Coleman[2] and Chandrakanth Bolisetti[2]

[1]Structural and Seismic Engineering Section (SSES),
Bhabha Atomic Research Centre Trombay, Mumbai – 400 085
[2]Facility Risk Group,
Idaho National Laboratory, Idaho Falls, ID 83402, USA
*rbanerjee@barc.gov.in**

Abstract

Design Basis Ground Motion is generally defined on rock outcrop because, in general safety related nuclear structures are founded on rock. For sites at which the bedrock is very deep, these safeties related structures are founded on soil. Consequently, the behaviour of the foundation of structures resting on soil is very much different than on bedrock. Hence, seismic ground response analysis is required to develop a site-specific response spectrum for the design of important superstructures in the region. One-dimensional ground response analysis is a commonly used method to estimate the ground responses under earthquake excitation in both equivalent linear and non-linear domains for both low to high strains. To understand the above phenomena, tests on F-55 Ottawa sand have been performed in a large scale geotechnical laminar box (GLB) at the Buffalo State University, New York. In this study, these tests have been simulated using numerical procedures involving equivalent linear and nonlinear time history analysis (using hyperbolic stress strain curve) using the author's in-house code which is limited to low to medium strains. The developed code, when tested for high strains, results in response accelerations that are lower than the experimental observations. The limitation of the model is that it predicts higher damping under larger strains. To match the damping under large strains, a modification is introduced in the developed nonlinear model which takes into account the above problem. With this modification, the predicted accelerations are in line with the experimental observation. Further, a study illustrating the performance of hyperbolic and multilinear backbone curves are studied based on the generation of the amplitude of high frequency harmonics in the response of nonlinear soil at high degree of nonlinearity. It is observed that the amplitude of odd harmonics is dependent on the number of parallel springs (or number of points) chosen for generating the multilinear

stress strain curve and it is least (minimum) if a continuous (hyperbolic) backbone curve is chosen for conducting the nonlinear analysis of soil column. In addition, the results of the dynamic model tests are compared with the results from a plane strain finite difference program in terms of acceleration time history at the top and bottom accelerometer locations and it is found out that the numerical predictions are in reasonable agreement with the experimental observation using hyperbolic nonlinear stress-strain soil model.

.

Keywords: ***Laminar Box, Pure shear boundary, Nonlinear, Equivalent linear.***

CONTENT

List of Figures

List of Tables

1. INTRODUCTION

Design Basis Ground Motion is generally defined on rock outcrop because, in general the safety related nuclear structures are founded on rock. For sites at which the bedrock is very deep, these safety related structures are founded on soil. Consequently, the behaviour of the foundation of structures resting on soil at different locations is very much different than on bedrock. This is because of irregular soil layering in space which leads to the different free field motions at different locations (for example, basin effect, one example of topographical effects in site response analysis)is shown in (Fig.1) [27],

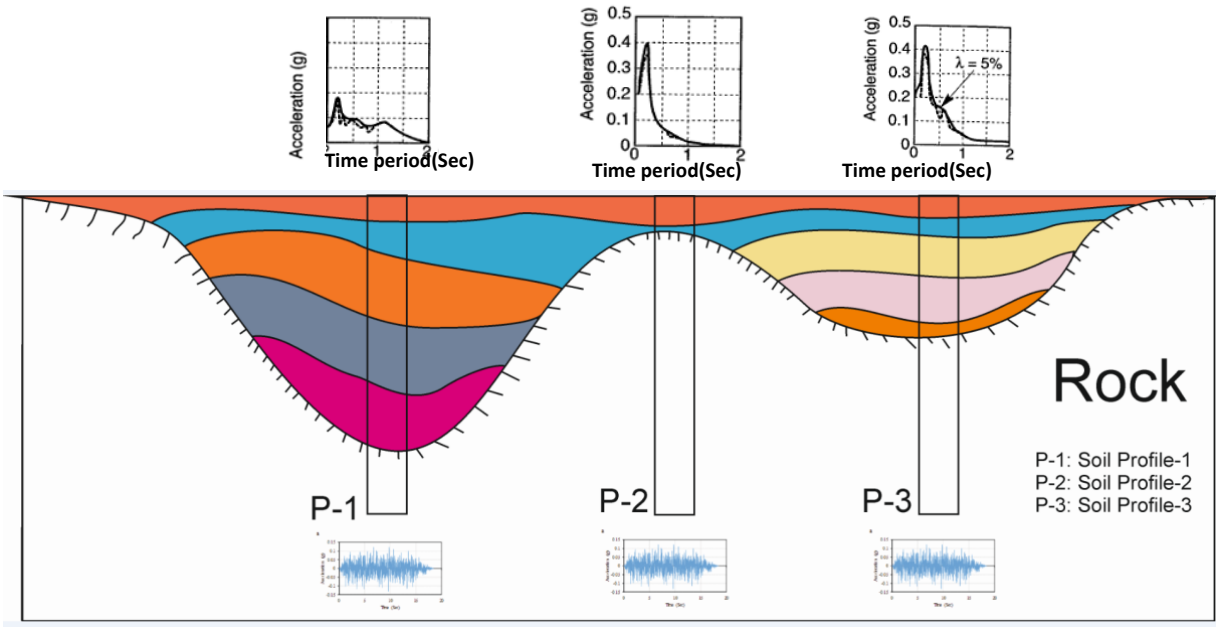

Fig.1. Variation of free field ground motion due to irregular topography irregularity in soil/rock profile.

This figure illustrates the point which has been stressed upon that there is a variation in the free field motion (and its frequency content) from one location to another. It is observed that where the soil depth is more, the response contains more lower frequency contents (or large time periods) as compared to the location where the soil depth is shallow. Hence, one solution to the problem is to model the entire soil/rock domain in 2D or 3D and get the soil amplification at various relevant locations. This requires huge computing space and time consuming. Hence, one alternative way is to go for local soil amplification studies near the location where we need to construct a plant/building etc. This saves time and cost as well as the results obtained are of a reasonable accuracy. In this report, local site amplification studies have been performed in one and two dimension to understand the phenomena of soil amplification in equivalent linear and nonlinear domain. The one-dimensional ground response analysis is commonly used method to estimate the ground responses under earthquake excitation in both equivalent linear and non-linear domains. The idea behind performing the exercise in both the domains is to study the conditions under which the two methods produce consistent estimates of site amplification. To understand the phenomena of site response analysis, tests on F-55 Ottawa sand has been performed in a large scale

geotechnical laminar box (GLB) at the University at Buffalo, State University of New York [7]. These tests have been further validated by numerical procedures involving equivalent linear and nonlinear time history analysis using our own in-house code, the description of which is provided in the following sections.

A2-D plane strain site response analyses have been performed by equivalent linear method and it is implemented in the in-house code for simulating the Laminar box tests conducted in the University of Buffalo, New York. A lumped mass model and pure shear boundary condition in equivalent linear domain, performing time-domain integration of the equations of motion step-by-step, has been utilised. It assumes that the soil layers are horizontal and the response of a soil site is predominantly due to the horizontally-polarized shear waves that propagate vertically from the underlying bedrock. An iterative procedure is used to obtain the values of the shear modulus (G) and the damping ratio (D) compatible with the representative effective shear strain in each soil layer. Though equivalent linear method is fast and provides reasonable estimates for most of the practical problems, it is an approximate solution to the actual non-linear seismic ground response. Hence, to compare the equivalent linear results, the actual non-linear response has been analysed by developing a 1-D total stress nonlinear model in time domain, in authors code for studying the behaviour of the soil column in a Laminar box. The method of analysis employed in time-stepping procedures can in some respects be compared to the analysis of a structural response to input ground motion [4 & 5]. The system is represented by a series of lumped masses or discretized into elements with appropriate boundary conditions. The system of coupled equations is discretized temporally and a time-stepping scheme, Newmark's β-method [20 & 21] is employed to solve the system of equations and to obtain the response at each time step. In addition, Masing rules [18] and extended Masing rules [24] are used in conjunction with the backbone curves to describe the unloading-reloading behaviour of a soil. For validating the developed nonlinear model at higher stains, shake table test was conducted at IIT Kharagpur and it was found that a slight modification is required to validate the model at higher strains. A small study illustrating the choice of backbone curve intended to be used in the time domain nonlinear analysis was performed and it was found out that the performance of hyperbolic backbone curve is much better in predicting the responses at all the frequencies than the multilinear model, and is recommended to be used in site response studies.

2. EXPERIMENTS CONDUCTED ON LOW STRAINS IN A SOIL COLUMN

A large scale geotechnical laminar box (GLB) at the Buffalo State University, New York [7] have been utilized for conducting experiments on F-55 Ottawa sand. The GLB is composed of 40 laminate rings stacked on top of each other and separated by ball bearings. The laminates are free to move laterally due to the frictionless bearings thereby allowing shear deformation of the soil contained within the box, which is numerically implemented by pure shear boundaries in this study. The box is lined with a custom 2.67 mm thick assembly of Firestone EPDM rubber. This rubber liner contains the soil material inside the GLB and prevents spillage of soil through the bearing-gaps between laminates. A uniaxial motion in the form of a sinusoidal wave or actual earthquake motion is applied at the bottom of the GLB by actuators. The motion applied to the GLB base propagates up through the soil

column within the GLB to the free top surface of the box. The interior dimensions of the GLB are 4.97 m in E-W direction, 2.74 m in N-S direction and 6.09 m in height. Each laminate including space for the bearings is 0.1524 m in height. There are 40 such laminates in the box. The box is filled with the sand up to a depth of 5.2 m. The experimental setup of the geotechnical laminar box is shown in (Fig.2).

Fig.2. Geotechnical laminar box test setup (Coleman et al., 2016).

2.1. Description of a Laminar Box

To correctly model a problem of one-dimensional (1D) shear wave propagation through an infinite soil layer in a dynamic centrifuge test, the following three criteria for the model container are: (1) the container must maintain a constant horizontal cross-section during shaking; (2) the container (ideally) must have zero mass and zero stiffness for horizontal shearing; and (3) the container must develop complementary shear stresses on the end walls of the container that are equal to those present on the horizontal surface. A special type of container known as a laminar container is developed which contains stack-ring devices, originally developed for simple shear tests, used to simulate free boundary conditions in earthquake modelling of soil deposits. The GLB container does not satisfy 2 and 3, which is why some boundary effects are to be expected during the test. (Fig.3(a&b)) demonstrates the discrepancies between the boundary conditions in a semi-infinite half space and in a model within a “rigid smooth wall container” during 1D shaking.

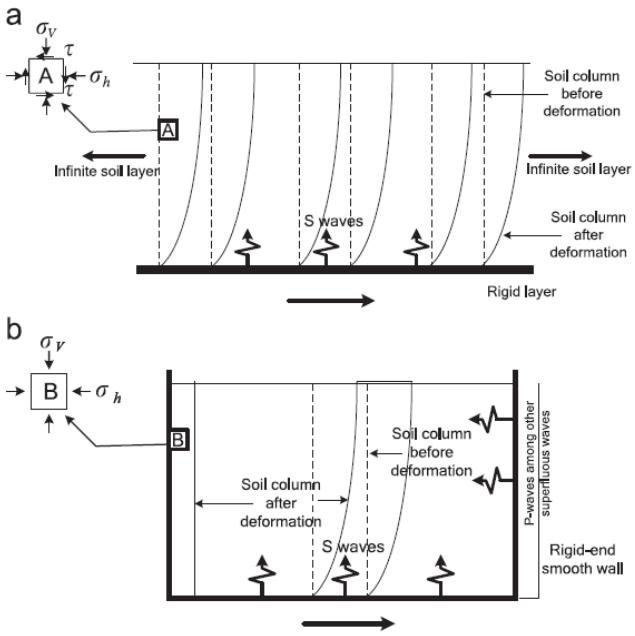

Fig.3(a)-(b). Boundary conditions in a 1-D shaking for (a) a semi-infinite half space and (b) a rigid wall container.

The mass of the stacked rings relative to the soil mass in the laminar box is not sufficiently small to be neglected (requirements of the 2nd and 3rd criteria). In addition, incompatible displacements (strain dissimilarity) between the zigzagged wall face and the soil bed as shown in (Fig.4) might cause P-waves among other superfluous wave reflections on both sides of container no matter which direction the soil bed moves to.

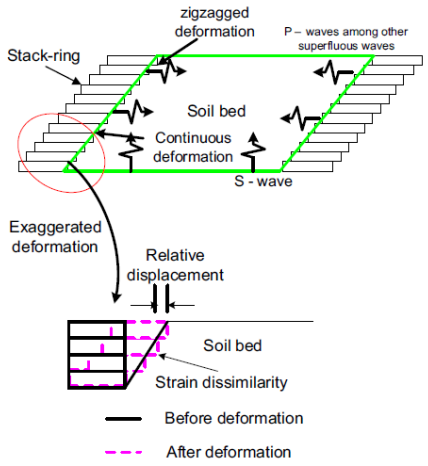

Fig.4. Incompatible displacement (strain dissimilarity) between the end wall oflaminar container and the soil bed during shearing.

But these two effects are quite less in comparison to "rigid smooth wall container" hence, this type of container is preferred than the former one. One can use the "rigid smooth wall container" but with absorbing materials (thermocol, duxeal, etc.) on the two sides of the container to reduce spurious P-wave reflections but with less effectiveness than the laminar box. The Ottawa F-55 sand is medium grained sand with the mean particle size (D_{50}) equal to 0.258 mm and contains less than 1% fines. The sand grains are mainly rounded, colourless

pure silica (silicon dioxide) uncontaminated by clay, loam, iron compounds, or other foreign substances. The maximum and minimum void ratios of the sand are 0.800 and 0.608, respectively [30] and [22]. The Ottawa sand is pumped into the GLB using hydraulic slurry processes [7]. Instruments like accelerometers are placed inside the GLB at different depths to enable measurement of real time soil shear wave velocity as it propagates through the soil column.

For measurement of real time shear wave velocity of the soil, the accelerometers are placed at different depths along the depth of the soil column and the first arrival time of the S-wave at each accelerometer is recorded. The time difference between two arrival times for accelerometer is noted and is divided by the distance between them to get its shear wave velocity. This exercise is repeated at each depth to get the profile of shear wave velocity. A schematic diagram illustrating the locations of accelerometers at different depths in the soil is shown in (Fig.5) and (Table.1).

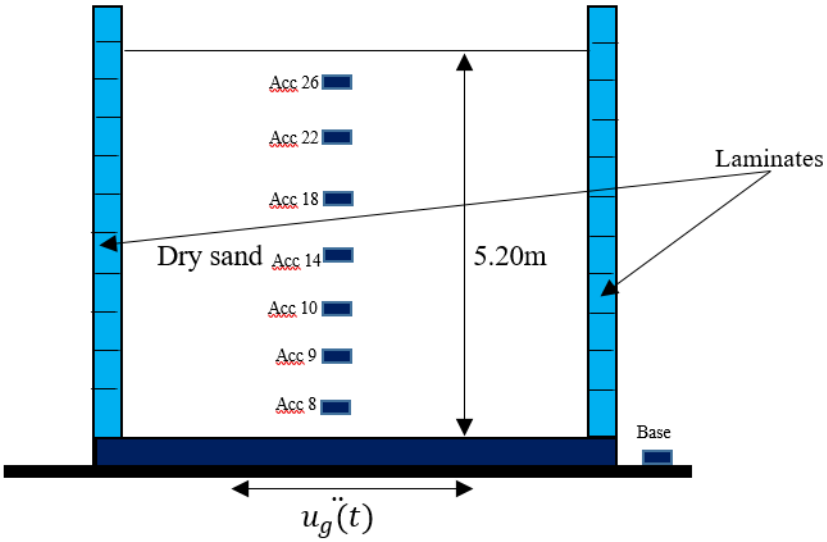

Fig.5. A schematic diagram of soil column in laminar box with accelerometer locations.

Table.1. Locations of the accelerometers within the GLB.

Accelerometers	Height above the base (m)
ACC 26	4.069
ACC 22	3.459
ACC 18	2.849
ACC 14	2.239
ACC 10	1.630
ACC 9	1.020
ACC 8	0.410
Base	0

2.2. Estimation of Shear Wave Velocity Profile with Depth of F-55 Ottawa Sand

To get the average shear wave velocity profile with depth, more than 25 tests have been conducted at 9 Hz, 8 Hz and 6 Hz input motions with a PGA of 0.03 g. For illustration purpose, the determination of V_s at a depth of 2.849 m is shown below.

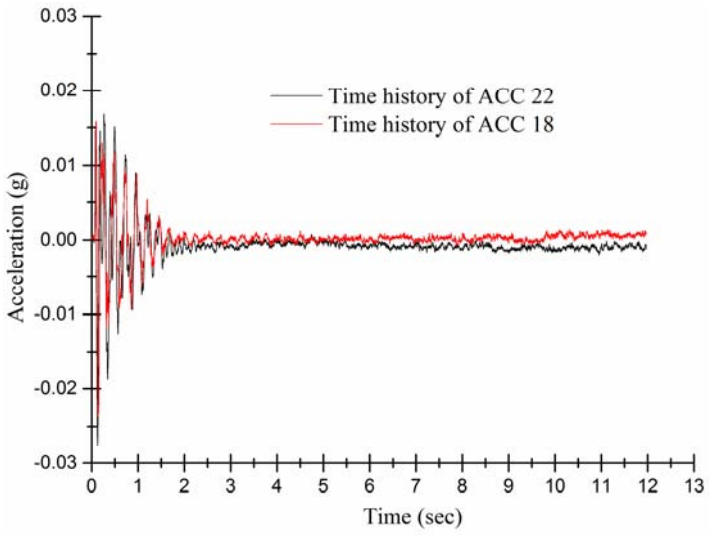

Fig.6(a). Recorded time history of ACC 18 and ACC 22 in Laminar Box test.

The entire time history of ACC 18 and ACC 22 is shown in (Fig.6(a)) above. For finding the arrival time of the waves for each of the accelerometer readings, the enlarged view of the initial portion of the accelerometer reading is shown in (Fig.6(b)) and the time difference of the wave arrival time is found to be 0.005 sec.

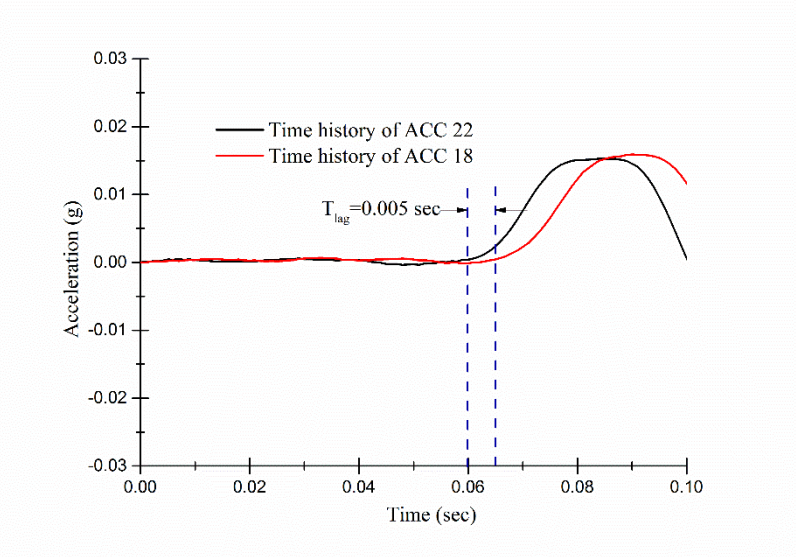

Fig.6(b). Enlarged view of the recorded time history of ACC 18 and ACC 22.

Kindly note here that the sample rate at which the data is recorded is pretty high (1000 samples/sec). As the sample rate is 1000 Hz, your time difference can only be multiples of 0.001. So if the real time difference is 0.0043, one can only can only see 0.004 or 0.005, which introduces an error in the shear wave velocity calculation. This is a disadvantage of

this kind of calculation, and needs to be mentioned here. One could also mention that if such a calculation is used, it is advantageous to use sensors with very large sample rate for better accuracy. Keeping these things in mind, the corresponding shear wave velocity of the soil is found to be V_s= (3.459-2.849)/0.005 =122 m/s. This exercise is repeated for each of the 25 test and an average value of V_s is taken for this depth of the soil. For getting the entire profile of Vs with depth, the entire process is repeated for each depth of recording and the final shear wave velocity profile with depth of soil is shown below in (Fig.7).

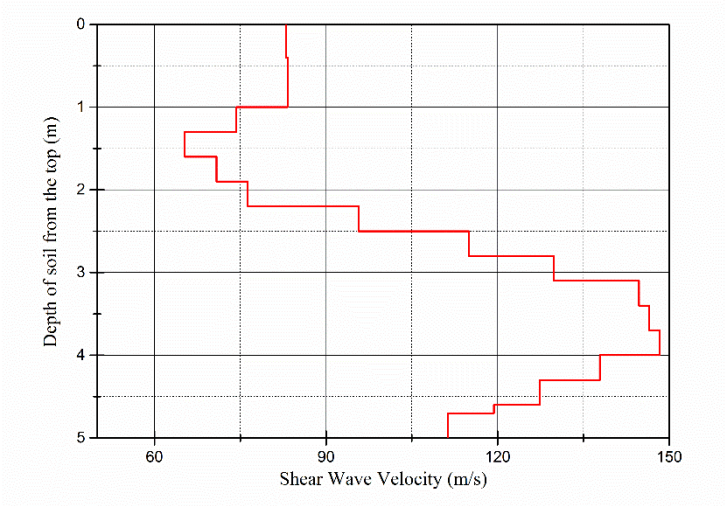

Fig.7. Shear Wave Velocity of soil with depth of soil in a laminar box test.

It is observed that the shear wave velocity of soil is smaller near the bottom. This is because earlier the the laminar box is filled by mixing the soil with water and pumping it into the box. This is the reason there is water in the box and the water was not fully drained from the laminar box due to which the degree of saturation was nonzero during the test. It is also observed that there is a dip in the shear wave velocity at a depth of 1.5 m which might be due to improper compaction. Using the above soil shear wave velocity profile, the numerical models developed during this study are validated with one such base motion chosen which has a peak amplitude of 0.03 g and a peak spectral acceleration at 9 Hz frequency. The recording of the time history has been done for 12 secs (shown upto 4 secs) and is shown in (Fig. 8(a&b)) in both time and frequency domains.

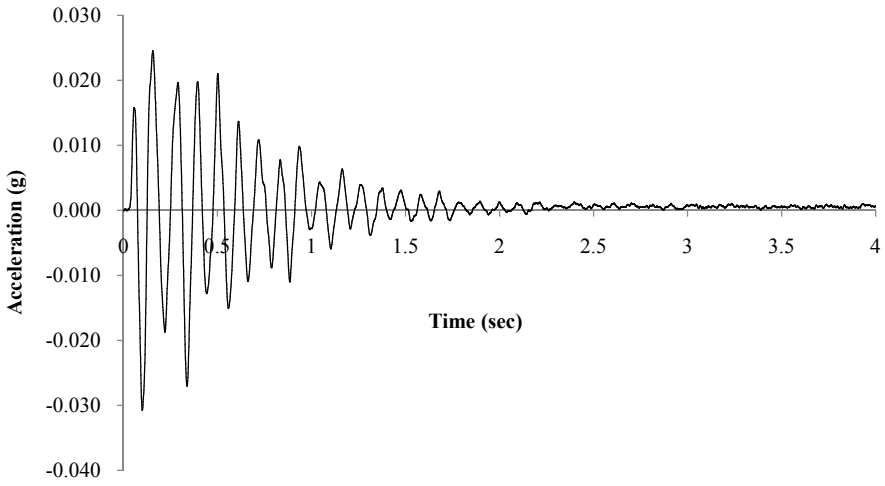

(a)

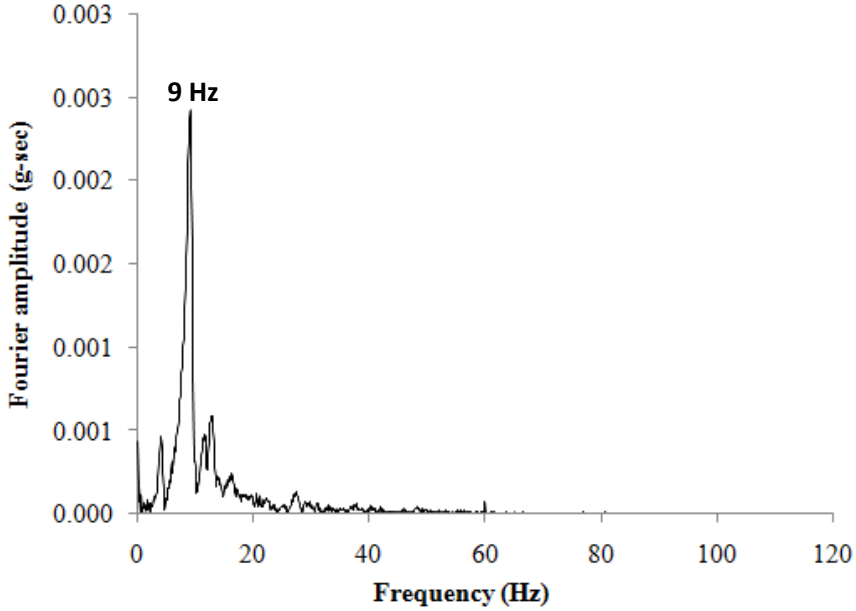

(b)

Fig.8. Applied base motion to the laminar box in both time and frequency domains.

To capture the strain dependant dynamic properties of F-55 Ottawa sand which will be utilised in the equivalent linear and nonlinear soil model described in the next section, torsional resonant column laboratory test (RCT) is conducted on the same soil sample for two different confining pressures (13.8 kPa and 55.16 kPa). The tests are done on a soil sample of 10.77 cm in height with an initial diameter of 5.07 cm. The type of sand is SP and its relative density is 58%. The specific gravity of sand is 2.65 with an initial void ratio of 0.61. The dry unit weight of the sand is 15.90 kN/m^3. The experimentally calculated curves of the normalised stiffness and its corresponding damping ratio of the Ottawa sand are shown in (Fig.9(a&b) below.

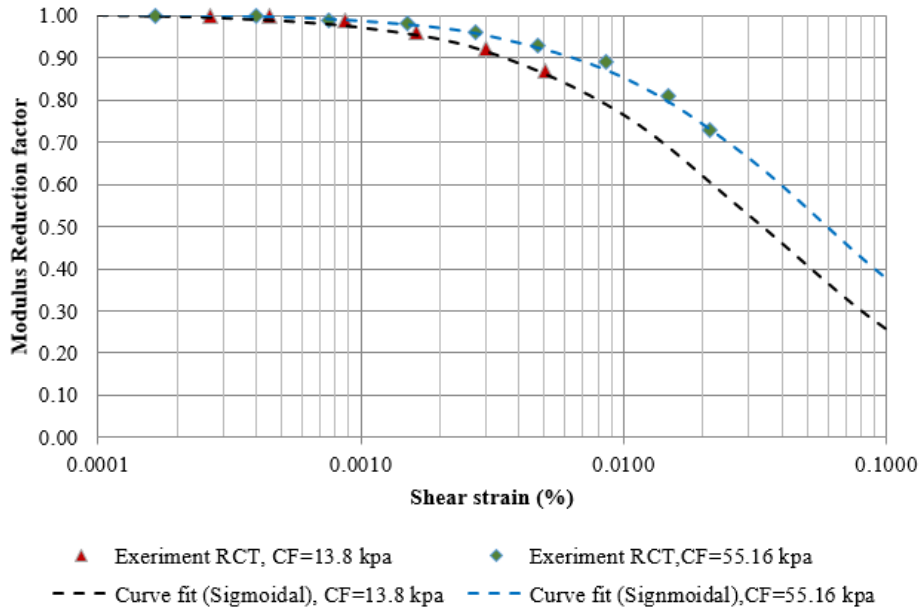

(a)

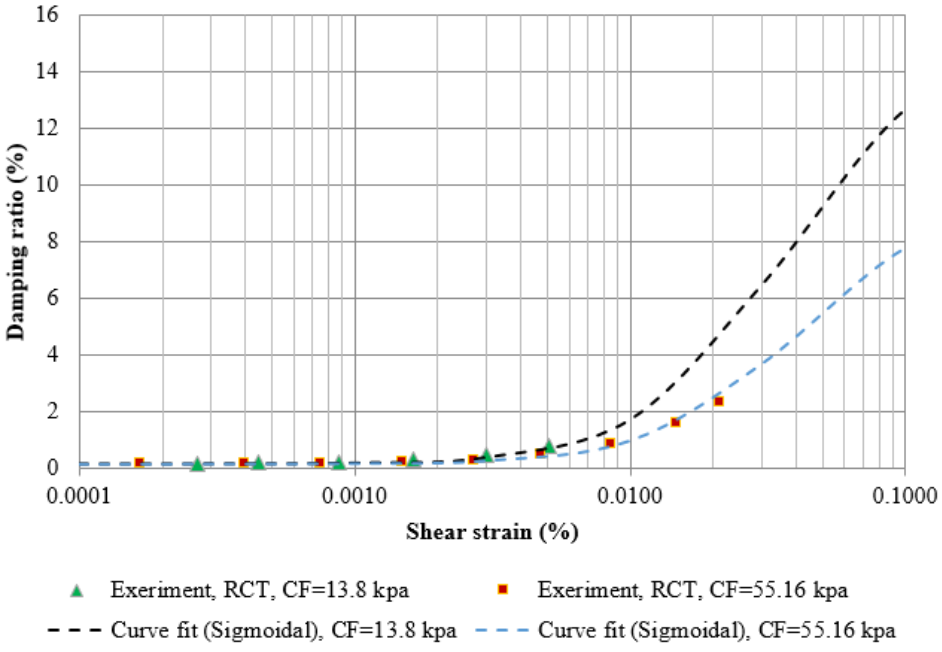

(b)

Fig.9. Variation of (a) normalised stiffness and (b) damping ratio versus shear strain for F-55 Ottawa sand by torsional resonant column tests (RCT).

3. ANALYSIS AND NUMERICAL SIMULATION OF LOW STRAIN TEST

An in house finite element program is developed for studying the soil response in a Laminar box by performing 2-D equivalent linear analyses in time domain and using Multi-point constraint [1] boundary condition. The lateral boundaries of the soil domain should reduce the unwanted reflections from the boundaries which is achieved by constraining the

boundaries to move in pure shear which in turn simulates a free field conditions. Further, a 1-D total stress nonlinear analysis of multiple degree of freedom lumped mass, spring and dashpot systems with appropriate boundary conditions has also been implemented in authors code to compare the results obtained from the equivalent linear analysis.

In the equivalent linear analysis, an iterative approach is followed [15], in which, the initial estimates of the values of the shear modulus, G_i and damping ratio, D_i, corresponding to small strains, are assumed for each soil layer. The estimated G_i and D_i are used to compute the ground response, including the time histories of shear strain for each layer. The effective shear strain in each layer is determined from the maximum shear strain in the computed shear strain time history. From this effective shear strain, new values for $G_{i+1}$and $D_{i+1}$are estimated for the next iteration. The above steps are repeated until the difference between the previous and the new values is less than 5-10%. The iteration converges within 3 to 4 steps, normally [26]. A flowchart illustrating the above approach is shown in (Fig.10(a)). In the equivalent linear approach, the following dynamic equation of equilibrium is solved in discrete time increments using time domain analysis.

$$[M]\{\ddot{u}(t)\} + [C]\{\dot{u}(t)\} + [K]\{u(t)\} = [M](I)\{\ddot{u_g}(t)\} \qquad \text{Eq.(1)}$$

where, (M) is the lumped mass matrix, (K) is the stiffness matrix, (I) is the influence matrix (equal to 1 in the direction of the application of motion, and 0 in the direction, where no motion is applied) and (C) is the damping matrix of the soil. The above equation is solved numerically at each time step using the constant average acceleration method.

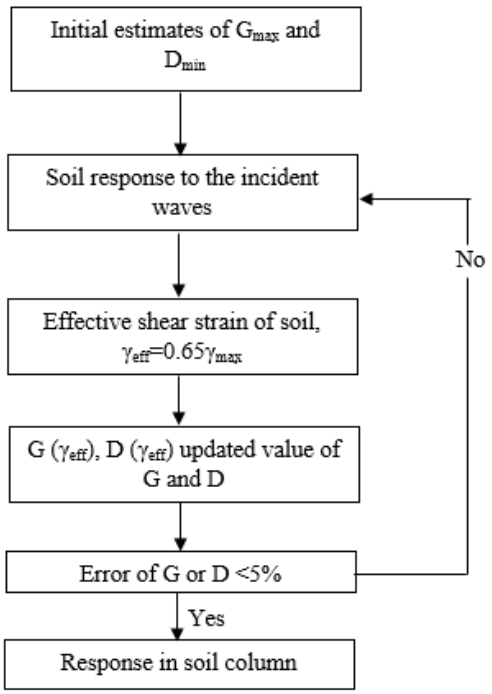

Fig.10(a). Flow chart of computational program for soil response analysis using equivalent linear method.

The base of the soil column is modelled as infinitely stiff. For the i^{th} layer of the soil, the soil mass is lumped at each node of an 8-noded, 2-D quadrilateral element (= ρV/8, where ρ is the density of soil, V is the volume of the element). The formulation of the stiffness matrix requires the following basic definition:

$$[K] = \int (B)^T [D][B] dv \qquad \text{Eq.(2)}$$

which in isoparametric formulation is expressed as:

$$[K] = t \iint_{-1}^{1} (B)^T [D][B]|J| d\xi d\eta \qquad \text{Eq.(3)}$$

where, η = y/a, ξ=x/a where 'a' is the half of the element size. 't' is the out of plane thickness of the element. (D) is the constitutive matrix in plane strain and given by:

$$[D] = \frac{E}{(1+\vartheta)(1-2\vartheta)} \begin{bmatrix} 1-\vartheta & \vartheta & 0 \\ \vartheta & 1-\vartheta & 0 \\ 0 & 0 & \frac{(1-2\vartheta)}{2} \end{bmatrix} \qquad \text{Eq.(4)}$$

in which, E is the elastic modulus and ϑ is the Poisson's ratio. For the formulation of the B-matrix, the following shape functions for an 8-noded element are defined:

$$N_1 = \frac{1}{4}(1-\xi)(1-\eta)(-\xi-\eta-1)$$

$$N_2 = \frac{1}{4}(1+\xi)(1-\eta)(\xi-\eta-1)$$

$$N_3 = \frac{1}{4}(1+\xi)(1+\eta)(\xi+\eta-1)$$

$$N_4 = \frac{1}{4}(1-\xi)(1+\eta)(-\xi+\eta-1)$$

$$N_5 = \frac{1}{4}(1-\xi)(1-\eta)(1+\xi)$$

$$N_6 = \frac{1}{4}(1-\xi)(1-\eta)(1+\eta)$$

$$N_7 = \frac{1}{4}(1-\xi)(1+\eta)(1+\xi)$$

$$N_8 = \frac{1}{4}(1-\xi)(1-\eta)(1+\eta) \qquad \text{Eq.(5)}$$

The node numbering in a single element is shown in (Fig.10(b)).

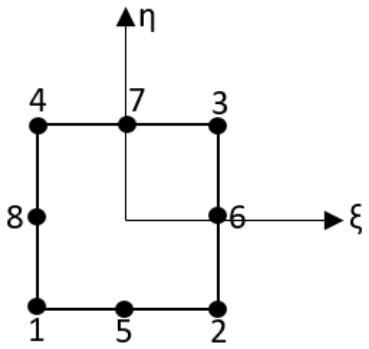

Fig.10(b). Node numbering in a 8-noded quadrilateral element.

The (C) matrix is a combination of elemental mass and stiffness matrices and is of the form [25]

$$[C] = \alpha_R[M] + \beta_R(K) \qquad \text{Eq.(6)}$$

The values of α_R and β_R are calculated by considering the predominant frequencies of input motion or soil column. In the equivalent linear analysis, the damping ratio is calculated with the variation of shear strain for a soil. For a frequency independent damping ratio, the formulation of damping for a multi-layered soil is followed as per [10]. The soil column is modelled using 2-D, plane strain, 8-noded, quadratic, quadrilateral element with two degrees of freedom (horizontal and vertical displacements) at each node. A rigid element is utilized to impose a multi-point constraint. A rigid element is a 2-D, bar element with high axial stiffness (AE/L=w) and two degrees of freedom at each node. It is connected to the two nodes of the lateral boundaries of the soil column. The axial stiffness is made high so that there is negligible axial strain in the bar element which implies that the deflection of the end nodes is same. One node acts as the "master" and another node acts as a "slave". The constraint equation that ties the horizontal and vertical degree of freedom is written in the following form [6]:

$$[B][u] = [A] \qquad \text{Eq.(7)}$$

where, B and A are constants. For homogeneous constraints, the value of (A) is equal to zero. The equation may be written in a modified form as:

$$[Q] = [B][u] - [A] \qquad \text{Eq.(8)}$$

(Q)=0 implies the satisfaction of the constraints. "Penalty augmentation" [6] is used for implementation of the constraints at the boundary degrees of freedom. Each multi-point constraint is viewed as the presence of a fictitious elastic structural element called penalty element (w) that enforces it approximately. This element is parametrized by a numerical weight. The multi-point constraints are imposed by modifying the assembled stiffness matrix which is submitted to the equation solver as:

$$[K_{modified}] = [K] + [B]^T w[B] \qquad \text{Eq.(9)}$$

If w =0, then the constraints are ignored, hence the selection of the appropriate weights are necessary to minimize ill-conditioned solution (with respect to inversion of the stiffness

matrix) as well as to avoid mesh locking. For instance, if we choose the horizontal nodal displacements at nodes 4 and 8, $u_{4x}= u_{8x}$, then it may be written as $u_{4x}-u_{8x}=0$, which is a homogeneous constraint. It may be written in the matrix form as:

$$[1 - 1]\begin{bmatrix} u_{4x} \\ u_{8x} \end{bmatrix} = 0 \qquad \text{Eq.(10)}$$

Where, $[B] = [1 - 1]$ and $[B]^T w[B] = w\begin{bmatrix} 1 & -1 \\ -1 & 1 \end{bmatrix}$

The above matrix is incorporated into the assembled stiffness matrix at the appropriate locations of the degree of freedom. It generally implies the addition of an axially rigid bar element with axial stiffness (w) to the two tied nodes. The trade-off value of weights is difficult to find, which will encompass all the problems. A rule is followed in which the weights are chosen typically on the order of 10^6 to 10^7 for double precision (64-bit processor) to avoid numerical difficulty [6]. At the bottom of the model, "rigid" base is assumed and the formulation is done in terms of total displacements. It may be noted that this traditional approach assumes that the total motion at the foundation base is known in terms of acceleration and the boundary degrees of freedom for the relative displacements are constrained to zero [37].

The present nonlinear model in the authors code is based on total stress analysis of multiple degree of freedom lumped mass systems with appropriate boundary conditions. The system of coupled equations, as shown in (Eq.1), is discretized temporally and a time-stepping scheme such as the "Newmark Average Acceleration" method [20] is employed to solve the system of equations and to obtain the response at each time step. The formulation of stiffness and damping matrix for lumped mass systems is the same as the one given in DEEPSOIL [11]. In this formulation for the viscous damping matrix, the value of stiffness matrix (K) is not updated at each time step which implies that the viscous damping matrix is not updated at each time step. To capture the hysteretic damping in the system, the rules of loading-unloading cycles are followed as proposed by [18] and [34]. As the extended Masing rules [24] and [31] cannot be converted into simple functional form, hence in this model, a modified dynamic stress-strain relationship is used which simplifies the modelling of the extended Masing rules. The stiffness matrix (K) is assembled at each time step using the incremental properties of soil layers obtained from a constitutive model that describes the cyclic stress-strain characteristics (backbone curves) of the soil layer. The modulus reduction curves, whereby the dynamic modulus of soil decreases with strain, is used to define the backbone curves. In this model, the equation of backbone curve is given by (Eq.11).

$$\tau = \frac{\gamma}{A+B|\gamma|^s} \qquad \text{Eq.(11)}$$

Where, τ is the shear stress, γ is the shear strain, γ_{ref} is the reference shear strain, 's' is a curve fitting parameter **(=1.0 for low to medium strains)**, $A=1/G_{max}$ and $B=1/\gamma_{ref}/G_{max}$. The value of γ_{ref} is used to adjust the shape of the backbone curve to get a proper match with the modulus reduction and damping ratio curves of a soil. The rules followed for hysteresis loading-unloading behaviour of a soil to satisfy the Masing rules for irregular loadings is given in [34].

The base of the soil column is assumed to be infinitely stiff. Each individual soil layer is assumed to have a nonlinear spring (which considers for hysteretic damping), and a dashpot for simulating small strain damping in soil (which is optional to use in this model). The lumping the mass at each node of the soil column based on the adjacent upper and lower soil properties are used for the formation of mass matrix. The formulation of stiffness matrix is such that it is updated at each time increment, and the stiffness k_i for i^{th} soil layer is given as $k_i=G_i/h_i = (\tau(\gamma_i)-\tau(\gamma_i-\gamma_{i-1}))/(h_i(\gamma_i-\gamma_{i-1}))$, which shows that the value of tangent modulus, G is used to update the stiffness matrix at each solution step. The time step for solving the nonlinear program is decided by the results obtained by choosing different time steps and the optimum time step is selected for the problem in which the results (in terms of acceleration, shear strain, etc.) does not differ by more than 1% from the previous one. Generally, the solution time step depends on the integration algorithm, time step of the input motion, etc. and hence a time step of 0.001 sec is taken for this study since the prediction of soil behavior is quite accurate at this time step. The discretization of the soil column within the laminar box test for the numerical analyses in DEEPSOIL [11] and the authors code program for both equivalent linear and nonlinear analysis is shown in (Fig.11). The soil layer thicknesses are selected by considering the maximum frequency (f_{max}) of the shear wave that the model could logically respond to during earthquake loadings [16].One such calculation for element size is shown below in which the maximum frequuency of propagation through an element is taken to be 25 Hz. The element size calcualted as per the speed of the propagation of shear wave: $V_s=f\lambda$, where λ is the wavelenegth of the propagating wave. The wavelength λ,is calculated to be λ=74.3/25=2.92 m. For proper capturing of a harmonic wavelength, minimum of 3 points are required but in this study 10 points (or nodes) is utilised for capturing a wavelength of frequency 25 Hz, hence the corresponding element size os 2.92/10=0.292m (or ~0.3 m). The above procedure is followed for calculation of element size of the GLB soil column.

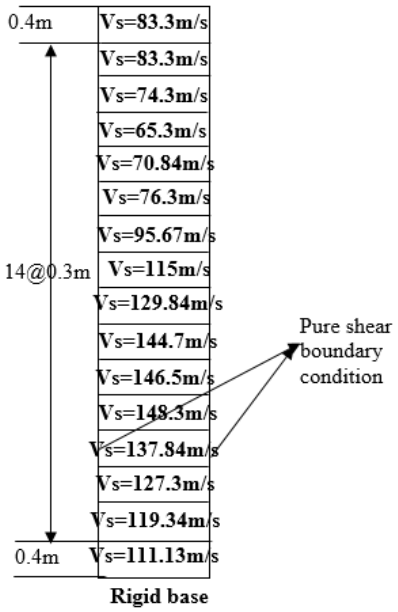

Fig.11. Numerical discretization of soil column in GLB test.

3.1. Calibrating the Backbone Curve of Soil From Strain Dependent Properties of Soil

In order to perform 1-D nonlinear time domain analysis, the strain dependant shake down strength (normalised stiffness) as well as damping ratio needs calibration and equations are fit for the experimental data for both normalised stiffness and damping ratio as given in (Eq.12 -15) for two different confining pressures.

$$\frac{G}{G_{max}} = \frac{1.005}{(1+\exp((-(\log_{10}\gamma)+1.479)/-0.4492)}$$, for confining pressure of 13.8 kPa Eq.(12)

$$\frac{G}{G_{max}} = \frac{1.005}{(1+\exp((-(\log_{10}\gamma)+1.229)/-0.4492)}$$, for confining pressure of 55.16 kPa Eq.(13)

$$D(\%) = 0.1514 + \frac{0.2733451}{(1.85+\exp(\left(-3.8597*\left((\log_{10}\gamma)+1.2882\right)\right))}$$, for confining pressure of 13.8 kPa Eq.(14)

$$D(\%) = 0.15014 + \frac{0.2833451}{(3.05+\exp(\left(-3.8597*\left((\log_{10}\gamma)+1.1082\right)\right))}$$, for confining pressure of 55.16 kPa Eq.(15)

These equations are useful for the calibration of backbone curve which will be utilised for nonlinear analysis of soil. The hysteretic form of the Kelvin-Voigt model consists of a spring (of stiffness k) and a dashpot (of viscosity η) connected in parallel (Kramer, 2005). Thus, the strain, γ, is imposed equally on the two elements and the corresponding stress, τ, has two components, one acting on the spring, τ_{spr} = G u(t) and another one on the dashpot, τ_{damper} = $\eta u(\dot{t})$, where u(t) is the shear strain of the soil. Combining these two resistances, the final expression for stress is given as:

$$\tau(t) = Gu(t) + \eta u(\dot{t})$$ Eq.(16)

For a harmonic excitation of the form, $F(t) = F_o \sin(\omega t)$, the response (in terms of displacement) is also of the form $u(t) = u_o \sin(\omega t)$ and the velocity is

$u(\dot{t}) = \omega u_o \cos(\omega t)$. The final expression may be expressed as:

$$\left(\frac{u(t)}{u_o}\right)^2 + \left(\frac{u(\dot{t})}{\omega u_o}\right)^2 = 1$$

Or, $$\left(\frac{u(\dot{t})}{\omega u_o}\right)^2 = 1 - \left(\frac{u(t)}{u_o}\right)^2$$

Or, $$\left(\frac{u(\dot{t})}{\omega u_o}\right) = \pm\sqrt{1 - \left(\frac{u(t)}{u_o}\right)^2}$$

Or, $\dot{u(t)} = \pm\omega\sqrt{u_o^2 - u(t)^2}$ Eq.(17)

Substituting, (Eq.17) into (Eq.16), the following expression for shear stress may be obtained.

$$\tau(t) = Gu(t) \pm \eta\omega\sqrt{\dot{u_o^2} - u(t)^2} \quad \text{Eq.(18)}$$

where, '+' is for the re-loading and '-' is for the unloading.

In the above equation, the term 'ηω' is replaced by '2Gξ'to make the expression frequency independent. Thus (Eq.18) may be expressed as:

$$\tau(t) = Gu(t) \pm 2G\xi\sqrt{\dot{u_o^2} - u(t)^2} \quad \text{Eq.(19)}$$

The above expression will give an ellipse for a value of shear modulus (G) and damping ratio (ξ). To incorporate strain dependency of shear modulus and damping ratio into (Eq.19), the equation may be modified as:

$$\tau(t) = G(u_o)u(t) \pm 2G(u_o)\xi(\dot{u_o})\sqrt{u_o^2 - u(t)^2} \quad \text{Eq.(20)}$$

where, u_o is the amplitude of the shear strain. $G(u_o)$ and $D(u_o)$ are obtained from the curves of modulus reduction and damping ratio with shear strain. This equation gives the equivalent hysteretic hypothesis using the strain dependant Kelvin-Voigt model. (Eq.20) is used to define an appropriate linear soil column model of 1m height with a value of small strain shear modulus. An authors code is developed in which the base of the soil column is fixed and at the top of the soil, a sine wave of constant amplitude of strain is applied. The response is in the form of shear stress which produces an inclined ellipse with amplitude of strain. The exercise is repeated for all the shear strain amplitudes (ranging from 10^{-4}% to 1%). (Fig.12) shows the hysteresis loops for each model data point based on the equivalent linear model data. (Fig.12) also shows the backbone curve which is used for the nonlinear model shear stress versus shear strain curve.

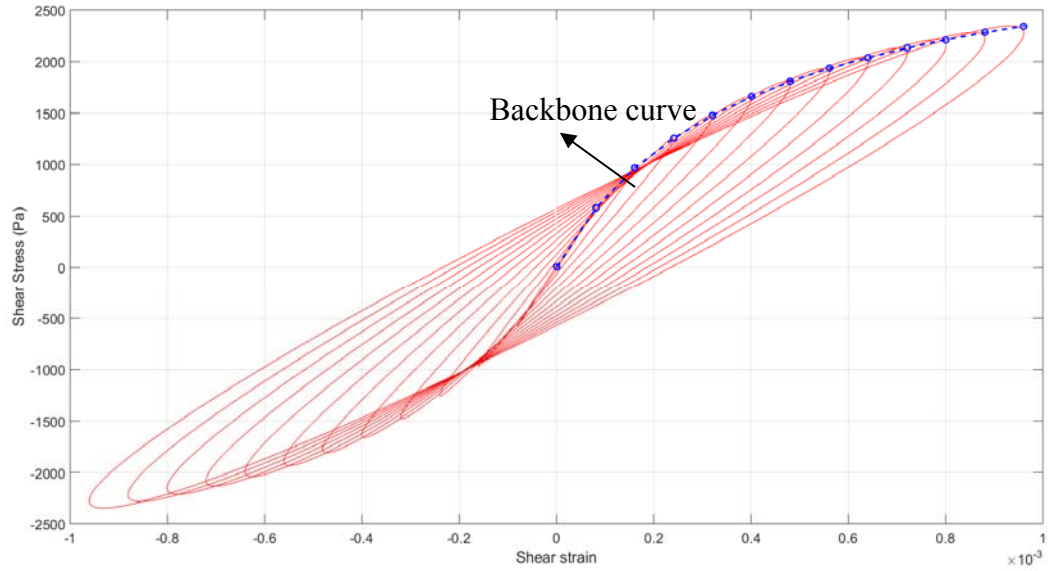

Fig.12. Variation of shear stress with shear strain in soil in a strain dependent linear Kelvin-Voigt model.

The equation of backbone curve (Modified MKZ model as per (Hashash and Park, 2002) to be used in the non-linear analysis of sandy soil is given by (Eq.21).

$$\tau(t) = \frac{Gu(t)}{1+\beta(\frac{u(t)}{u_{ref}})^s} \qquad \text{Eq.(21)}$$

where, β = 1.59, s = 0.66 and u_{ref} = 0.00092 for a sandy soil. Using the equation of the backbone curve with the above parameters, an authors code is developed which considers the unloading and reloading portions of the non-linear loops using the first two Masing rules [18]. Essentially, these state that (1) a new (but inverted) function is started upon reversal, implying that the initial unload modulus is G, and (2) the first quarter-cycle of loading is scaled by one-half relative to all other cycles [12]. The stress strain curves are generated by appliying a series of constant strain amplitde strain time histories at the top of the soil column of 1m in height as before. The stress-strain curve following the Masing rules is shown in (Fig.13).

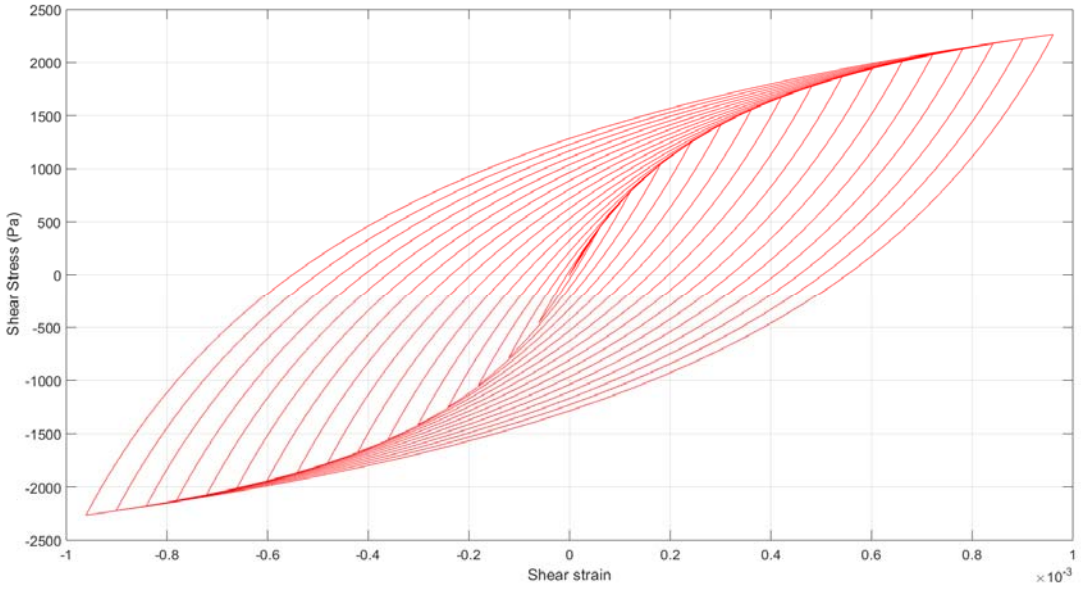

Fig.13. Variation of shear stress with shear strain in soil following first two Masing rules.

The material properties for the nonlinear model are defined to match the equivalent linear material properties (shown in (Fig.14(b)) as close as possible in terms of modulus reduction. The energy absorption for the lowest strain value (shown in (Fig.14(b)) is approximated by adding a low-strain (viscous) damping to the nonlinear model material properties. The calibration of the model in terms of the modulus reduction of a sandy soil with strain is shown in (Fig.14(a)). Though the match with modulus reduction curve is good, a deviation may be noticed in the damping ratio at higher strain levels (refer to (Fig.14(b)). It may be noted that a better match for damping is obtained at low strains, but for higher strains, the damping is overestimated. This may be also seen in (Fig.14(b)). This leads to an underestimation of shear strains as well as surface intensities in the form of PGA at the ground surface.

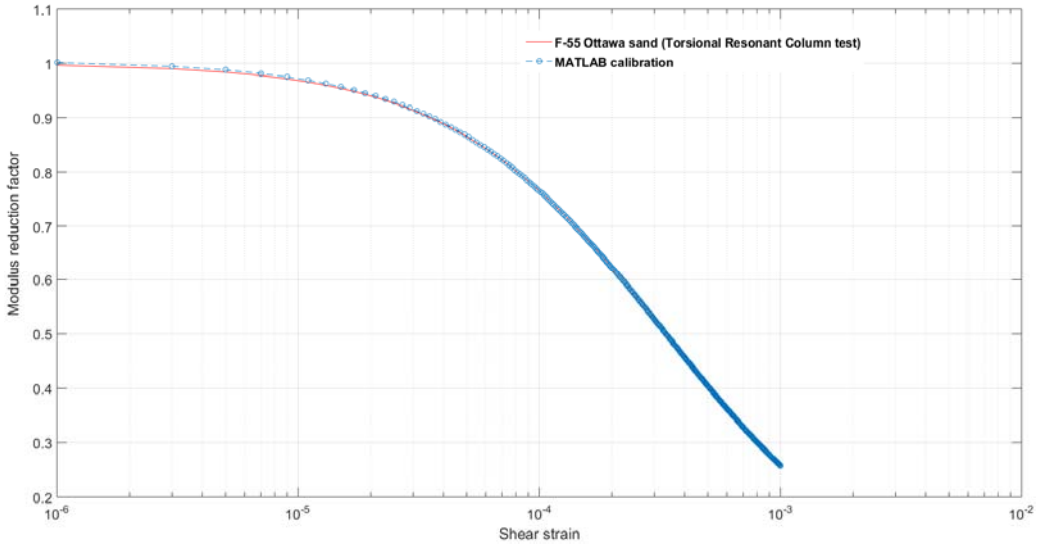

Fig.14(a). Comparison of shear modulus reduction with strain obtained from the authors code and that found in F-55 Ottawa sand.

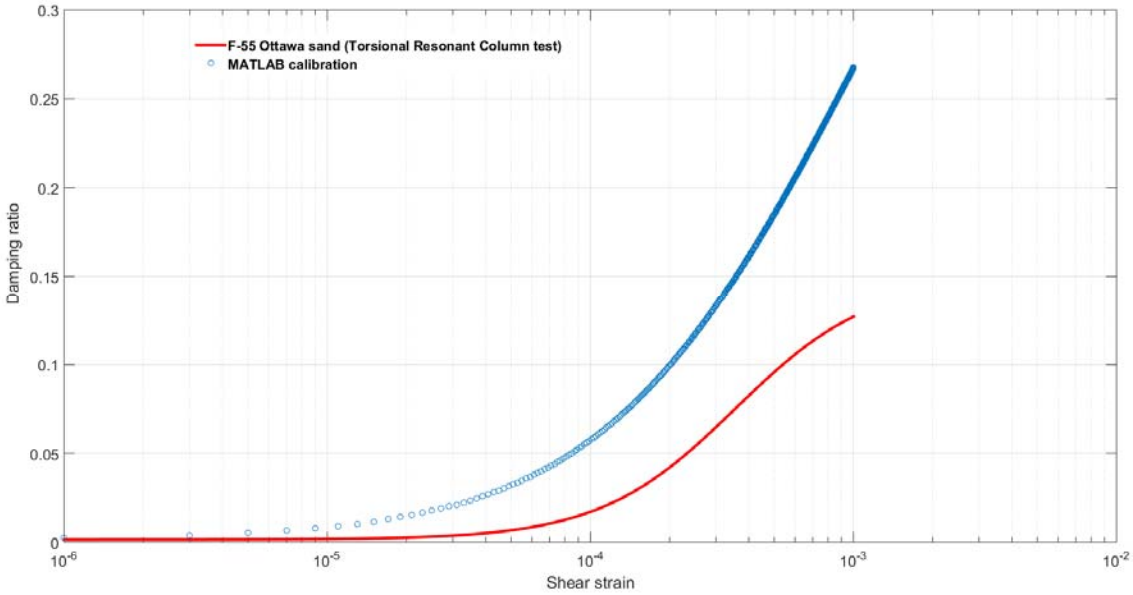

Fig.14(b). Comparison of damping ratio with strain obtained from the authors code and that found in F-55 Ottawa sand.

The energy absorbed per cycle for the soil column is calculated as the area of the hysteresis loop for each amplitude of shear strain. (Eq.22) shows a simple trapezoid rule for numerical integration that may be used if the shear stress and the shear strain are in tabular form [28 & 29],

$$E_{loop} = \sum_{j=1}^{N} \frac{\tau_j + \tau_{j-1}}{2} (u_{oj} - u_{oj-1}) \qquad \text{Eq.(22)}$$

The final parameters of the modified MKZ backbone curve for the F-55 Ottawa sand is given in (Table.2).

Table.2. The curve fit parameters for F-55 Ottawa sand (refer to (Eq.21)).

Type of Soil	B VALUE	S VALUE	U_{REF}
F-55 Ottawa Sand (CF=13.8 kPa)	1.52	0.976	0.000515
F-55 Ottawa Sand (CF=55.16 kPa)	1.46	0.975	0.00088

3.2. Results of the Numerical Simulation

After calibration with the stiffness degradation only disregarding the mismatch with the damping values at higher strains, the value of γ_{ref} (the reference shear strain) used for the hyperbolic model in (Eq.11) is found to be 0.059% and 0.0345% for confining pressures of 13.8 and 55.16 kPa, respectively. These backbone curves are used for the nonlinear analysis of F-55 Ottawa sand in laminar box tests. It is also validated against the results obtained from DEEPSOIL [11]. The small strain damping used for the non-linear analysis is taken to be 5%. The value of damping is taken on a bit higher side, usually a small strain damping of 1-1.5% is sufficient. The experimental validation of the model is shown in terms of variation of acceleration with depth for the specified base motion in (Fig.15(a)). The model predictions (equivalent linear and nonlinear) are compared with the test results and results obtained from DEEPSOIL [11] program. In addition, the numerical validation of shear strain with depth obtained from DEEPSOIL is compared with the authors code which is shown in (Fig.15(b)) below.

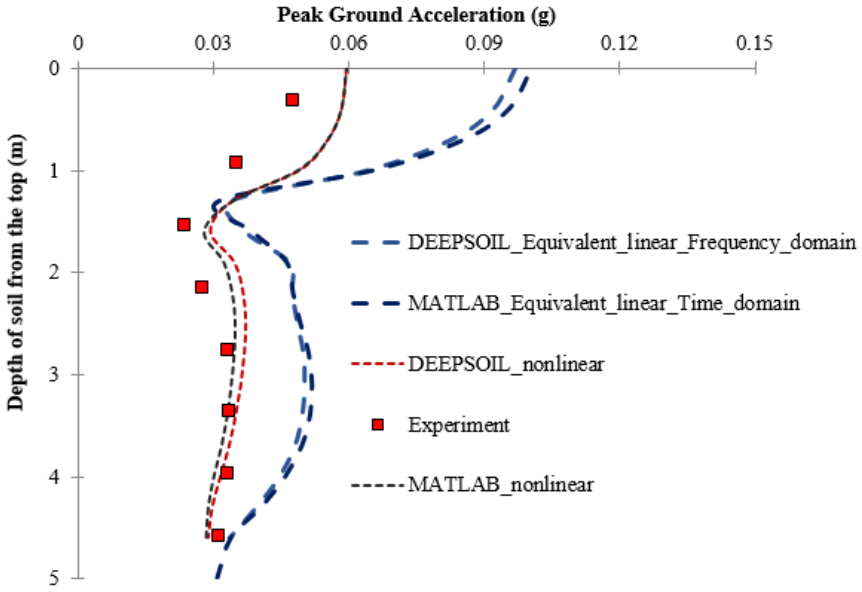

(a)

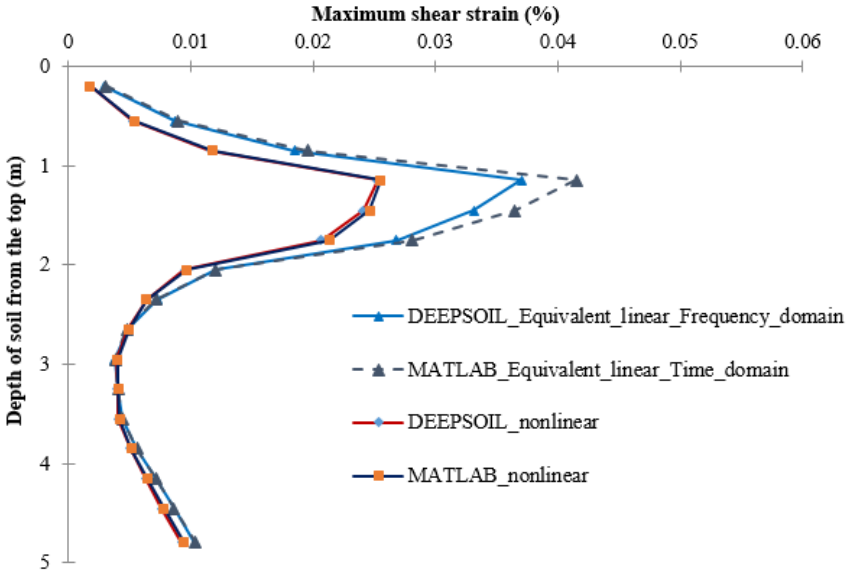

(b)

Fig.15. Comparison of the (a) peak accelerations and (b) Maximum shear strain with soil column depth in the GLB test for equivalent linear and nonlinear analysis.

From (Fig.15(a)), it is observed that there is a drop in the peak acceleration value around 3 to 4m depth. This is because of an interference of second mode of vibration in the soil column during the test which has a lesser amount of mass participation in comparison to its fundamental mode. This observation is also supported by comparing the acceleration time history in the frequency domain, both numerically and experimentally, for ACC 8 and ACC 14 (refer to (Fig.16)). Moreover, in comparison to equivalent linear analysis, the nonlinear analysis predicts closer results in terms of PGA with depth with the experimental observations [19].

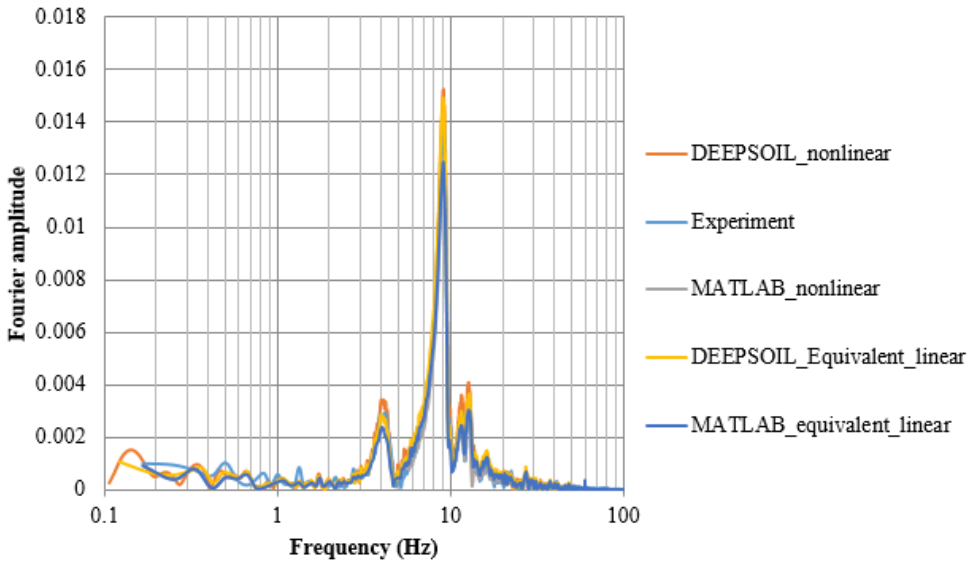

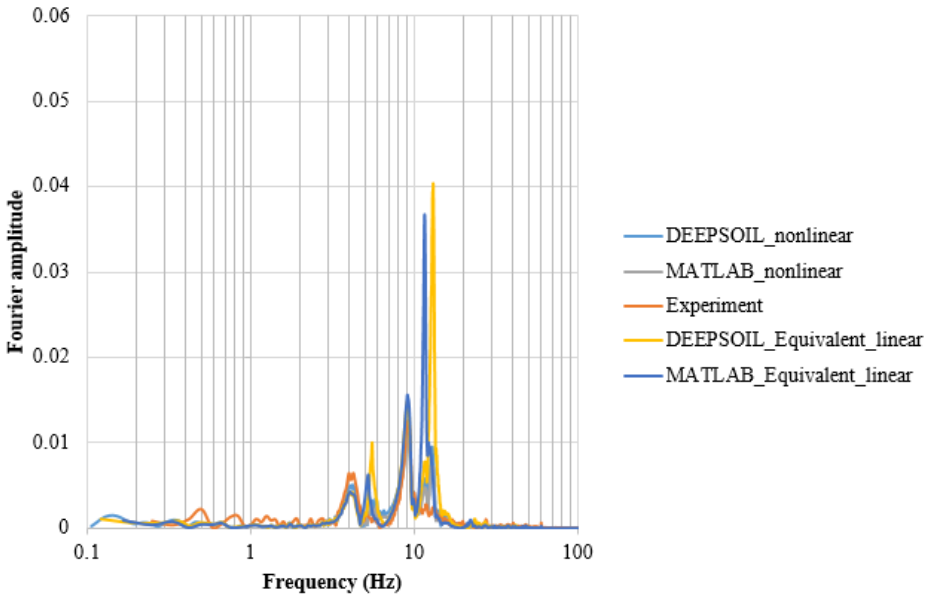

Fig.16. Fourier spectrum of ACC8 and ACC14 from GLB experiments, AUTHORS and DEEPSOIL(Hashash et al., 2012).

From the Fourier spectrum of ACC8 and ACC 14, it may be seen that there are three predominant peaks, the first one at 4.26 Hz, second one at 9Hz and the final one at 12.56 Hz. Out of these, the peak at 9 Hz is the frequency of the input motion, and the peaks at 4.26 Hz and 12.76 Hz are the two fundamental modes of vibration of the soil column. Hence the notion that the higher modes are occurring during the experiment is supported by these findings which also supports the fact of the de-amplification of peak accelerations as observed in (Fig.15(a)). The results obtained from the numerical analysis are in reasonable agreement to the experimental observations and demonstrate the numerical predictive capability of the developed model in equivalent linear and nonlinear domain. There are subtle differences in the frequency content especially between 10 and 11 Hz obtained from the responses of soil column in equivalent linear analysis from the authors code and DEEPSOIL. This may be due to the solution alogrithm followed by DEEPSOIL which does it in frequency domain and the authors code follows time domain. The deformations of the soil column at two instants of time obtained from the authors code for equivalent linear analysis are shown in (Fig.17),

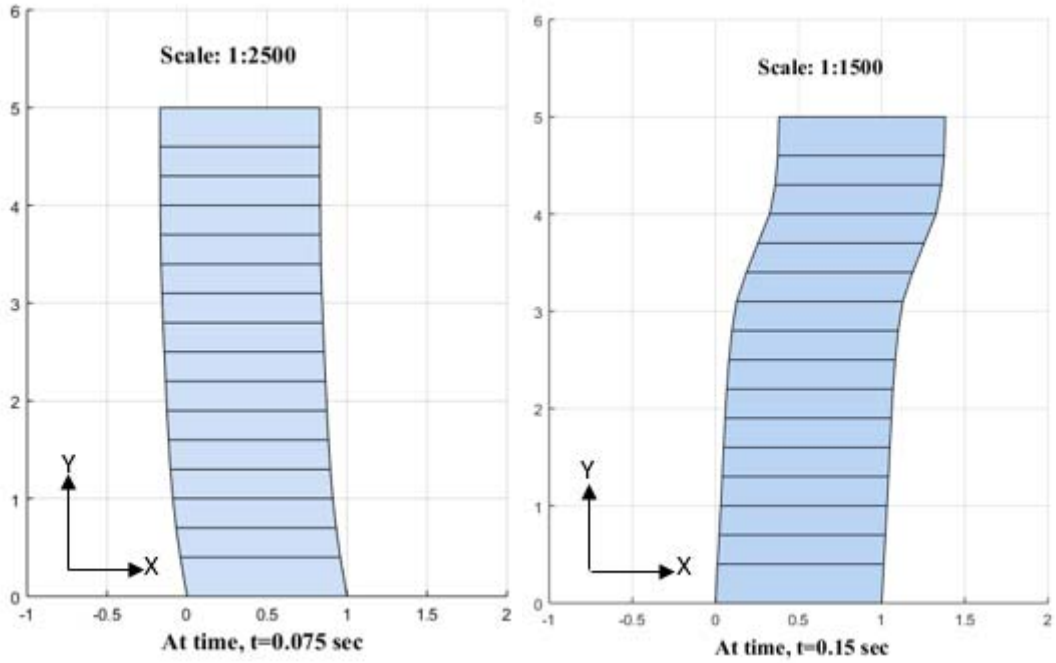

Fig.17. Deformations of the soil column at two time instants predicted by AUTHORS program.

From the deformed mesh at 0.15 sec, it may be observed that there is an influence of higher modes along with the fundamental modes of the soil column, which is dominant at a height of around 3-4.5 m. This is not observed in the deformed mesh at 0.075 sec in which the entire soil column is moving in its fundamental mode. This is also a supportive evidence of the de-amplification of peak acceleration at the concerned zone as shown in (Fig.15(a)). The small differences are due to the frequency domain technique utilized in DEEPSOIL [11] and the time domain technique (Newmark's β-method) utilized in authors code to solve the same problem in equivalent linear domain.

To validate the correctness of the stress-strain rules for nonlinear analysis, the shear stress vs. shear strains have been compared with DEEPSOIL and authors code at depths of 5 m and 1.3 m from the top of the soil surface (refer to (Fig.18)).

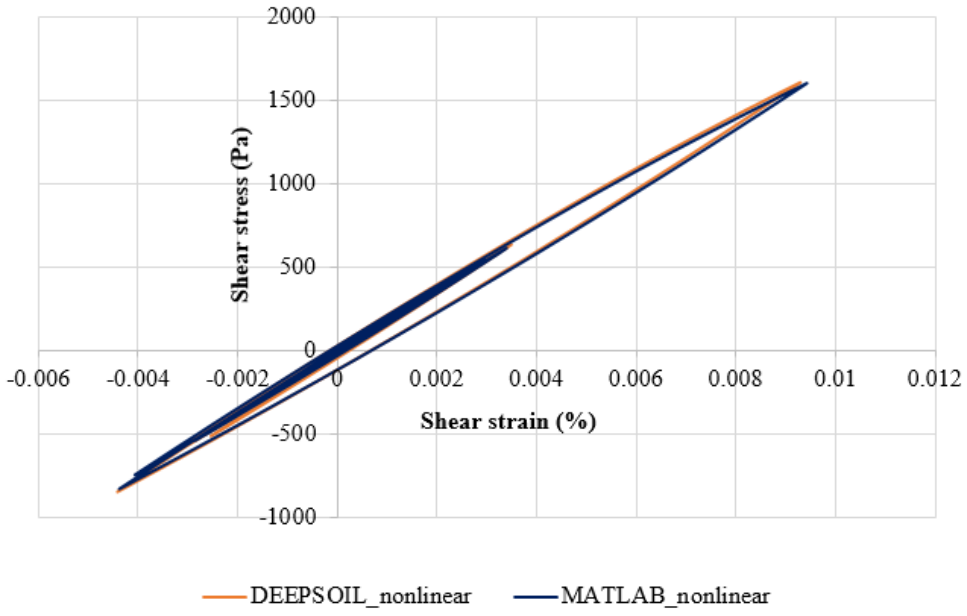

(a)

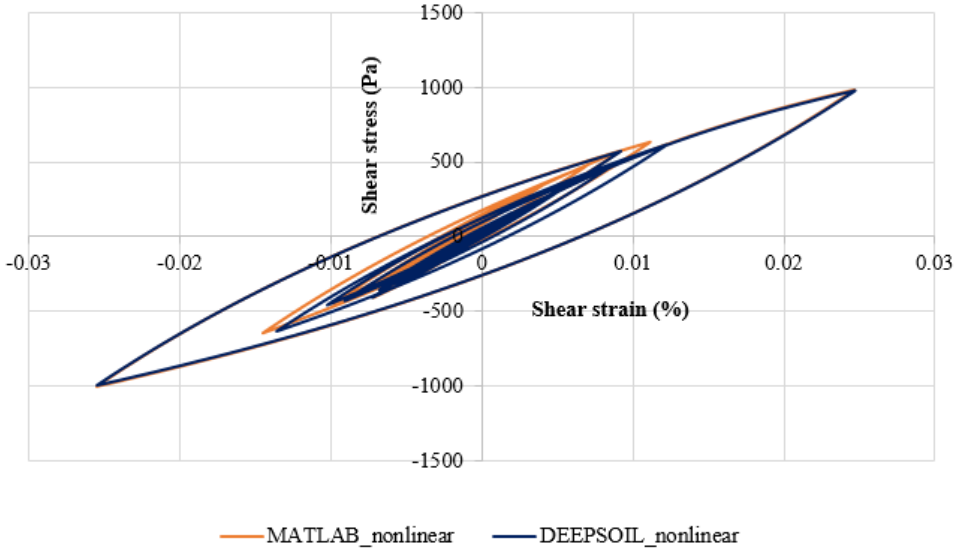

(b)

Fig.18. Comparison of stress-strain loops for soil column at a depth of (a) 1.3m, (b) 5.0m from the top of the soil surface.

It is seen that the stress-strain loops match reasonably well for depths of 1.3 m and 5 m. Thus, these results benchmark the nonlinear code. In a nutshell, it is seen that the nonlinear time domain analysis gives better results in comparison to equivalent linear analysis although it is time consuming hence, this methodology is preferred.

4. EXPERIMENTS CONDUCTED ON HIGH STRAINS IN A SOIL COLUMN

For validation of the developed model with "**higher strains (>1%)**", a uniaxial shake table test was conducted on dry Kasai river sand. The shake table essentially comprises of a 1m by 1m steel table mounted on rails. The load carrying capacity of the table is 5 ton. The table is attached to an actuator which vibrates the table in a uniaxial horizontal direction. The servo hydraulic actuator has a capacity of +/- 50 kN. It has a stroke length of +/-100mm. The actuator is driven by a controller which has a capability of accepting an actual earthquake (random, cyclic) loading as input and generating it between the frequencies range of 0.01 Hz and 50 Hz. The actuator has the capability to hold and restart the loading during a test. It has the facility to increase the base load, frequency and amplitude during a test. The model tests, reported here, are performed in a rigid plexiglass container of dimensions 0.8 m x 0.85 m x 1.0m (length x breadth x height) with top open. The plexiglass sheets are 16 mm thick and glued to each other as well as fixed in a steel frame consisting of steel angles.

The setup consists of dynamic shake table test of the 0.65 m high sand bed. In this case, the test container is filled with the dry sand at a uniform density of 1600 kg/m^3 (unit weight = 15.7 kN/m^3) up to the top, maintaining a 50 mm gap between the top of the test container and the top of the sand layer. Three accelerometers, one at the top of the soil, one near the bottom of soil and another one on the shake table, are placed as shown in (Fig.19),

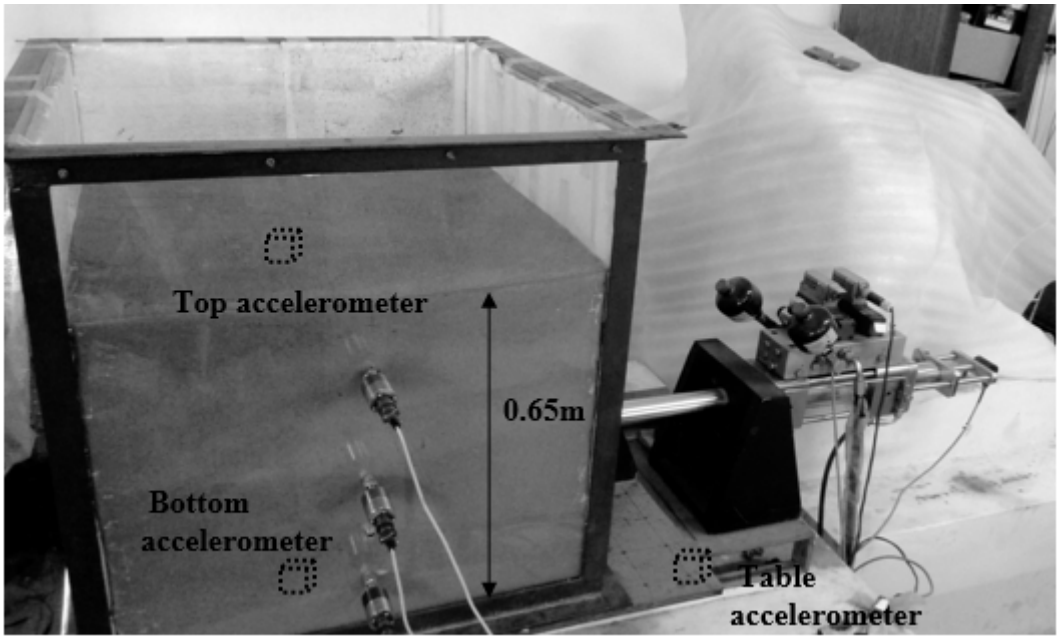

Fig.19. Test setup for dry sand testing under harmonic excitation.

One of the important challenges in the laboratory scale dynamic soil performance studies is to replicate the infinite boundary condition in the small test chamber. In a soil within a test chamber, as in this experimental study, the finite dimension of the soil layer does not allow the complete dissipation of the energy induced by the wave propagation. Moreover, the presence of the artificial boundaries induces the generation of P-waves which may add inaccuracies in the expected responses. The past studies by [3], [17] have demonstrated that the presence of foam sheets at the boundaries enables the dissipation of a certain amount of

energy. They have also demonstrated that higher absorption may be achieved using thicker sheets of foam. In the present study 32 mm thick thermocol sheets are pasted on the inner walls of the test container to reduce the reflection and the refraction of waves at the boundaries.

In this figure, the pore pressure transducers which are shown in the figure are removed before the commencement of the test. The front plexiglass wall of the container is lightly greased instead to allow viewing of the behavior of the foundation soil during the tests. The bottom of the container is made rough by gluing sand grains on the bottom to allow the generation of shear stresses at the bottom of the tank and to prevent any slippage [17]. The PGA amplification is found out by taking the ratio of the measured maximum (absolute) value of accelerations from the top and the bottom time history (motions applied to the shake table). The amplification of the motions through the sand is found to be 1.514 for the dry sand.

4.1. Properties of Kasai River Sand

A local uniform grained sand (Kasai River sand) is used in this study. The grain size distribution of the sand is shown in (Fig.20).

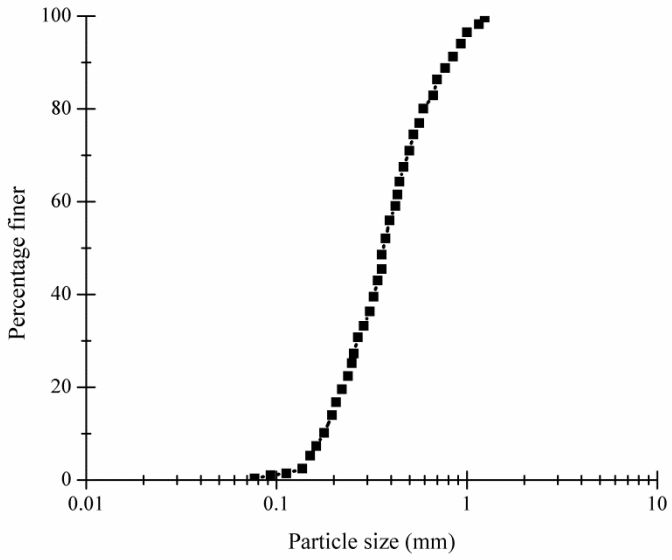

Fig.20. Grain Size Distribution of dry Kasai River sand.

It is classified as poorly graded sand (SP), according to the Unified Soil Classification System (USCS). The specific gravity of the sand is 2.72. The maximum dry unit weight $\gamma_{d(max)}$ is 16.7 kN/m^3, and the minimum dry unit weight $\gamma_{d(min)}$ is 14.03 kN/m^3. The uniformity coefficient (c_u) and coefficient of curvature (c_c) of the sand are found to be 2.84 and 0.87, respectively. In all the model tests, the bulk unit weight of the sand is maintained at 15.7 kN/m^3 and a relative density, D_r, of 67%. The drained triaxial shear tests are performed on the sand to find its shear strength parameters. The effective cohesion (c') and the effective angle of friction (φ') obtained from triaxial tests are 0.0 kPa and 32^0, respectively. Some of the previous studies [27] have shown that the shear wave velocity (or shear modulus) of a sand increases with depth because of an increase in the confining pressure. Hence, in this

study, a parabolic variation of the elastic modulus of Kasai River sand, as given below, has been assumed [12]:

$$E_0 = p_{ref} K_G \left(\frac{p'}{p_{ref}}\right)^n \quad \text{Eq.(23)}$$

Where p_{ref} is the reference pressure (=100 kPa), p' is the mean effective stress and K_G is a stiffness multiplier (=133.26, in the present case) and n is an exponent parameter (=0.45 in this case). The values of p_{ref} and K_G are obtained from the drained triaxial tests on the sand. (Table.3) shows all the material properties for the foundation sand.

Table.3. Material properties of Kasai river sand.

Parameters for the foundation sand	**Value**
Mass density(kg/m^3)	**1600**
Cohesion(Pa) (c')	**0**
Angle of internal friction, φ'	**32^o**
Stiffness Multiplier, K_G	**133.26**
Exponent, n	**0.45**
Poisson's ratio, ν	**0.3**

For studying the performance of dry Kasai river sand under high strains, the input motion of PGA 0.3503 g is applied for 7 sec. The acceleration time history recorded at the table top is shown in (Fig.21) for a predomainant input frequency of 2 Hz which is seen in the plot of frequency domain,

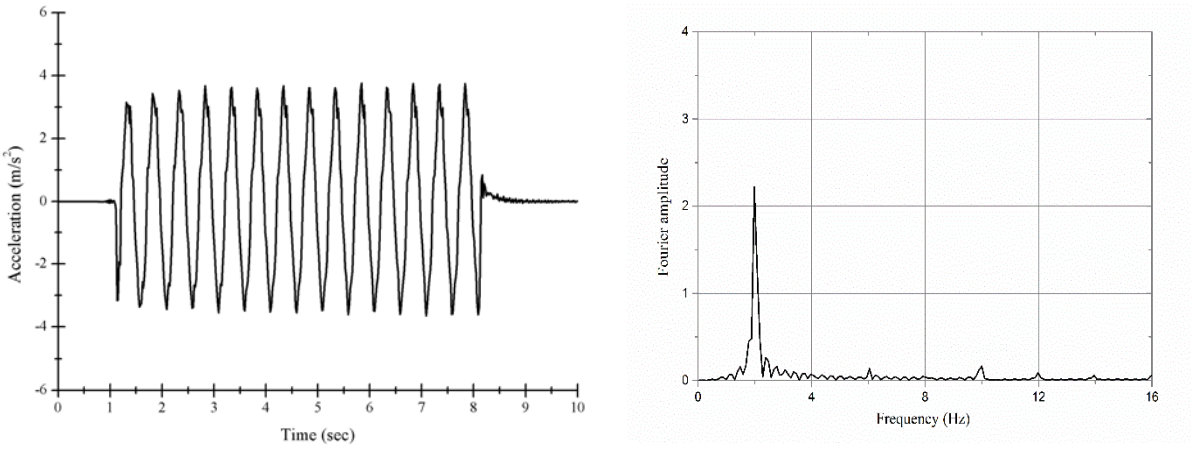

Fig.21. Input motion for dry sand on a shake table in time and frequency domain.

4.2 . Free vibration characteristics of Kasai River sand

Often the properties of a medium may be identified by letting waves propagate through the medium and studying the decrease in amplitude of the waves as the system is set into a state

of free vibration. A reduction in the amplitude of the wave is caused due to the internal damping of a soil within the mass of the material. Hence, the natural frequency of the soil column is also found experimentally from the free vibration portion of the accelerometer readings near the top surface of the sand bed as shown in (Fig.22(a)),

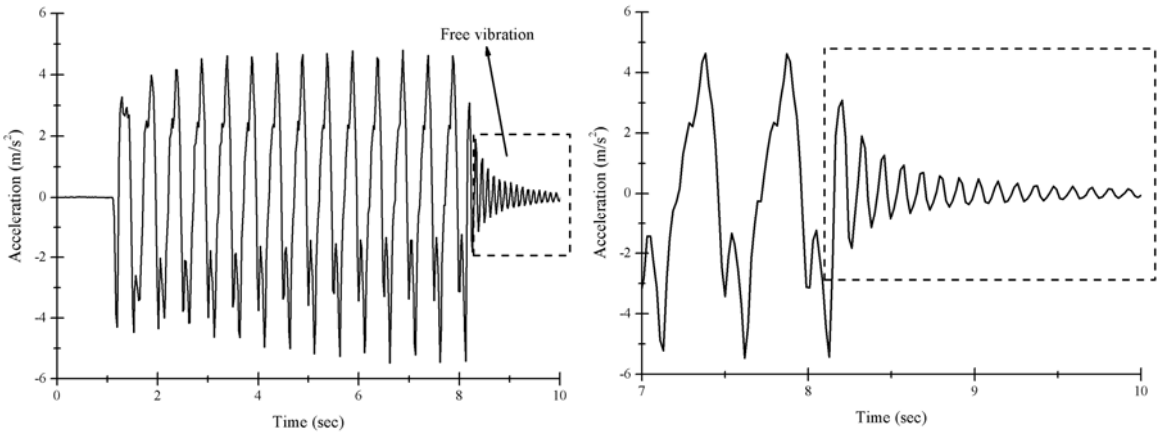

Fig.22(a). Acceleration time history near the top of sand bed and (b) close view of free vibration response of dry sand.

A close view of the free vibration portion of the motions is shown in (Fig.22(b)). (Fig.23(a)) shows the accelerometer readings in the frequency domain from where the natural frequency of the soil is obtained.

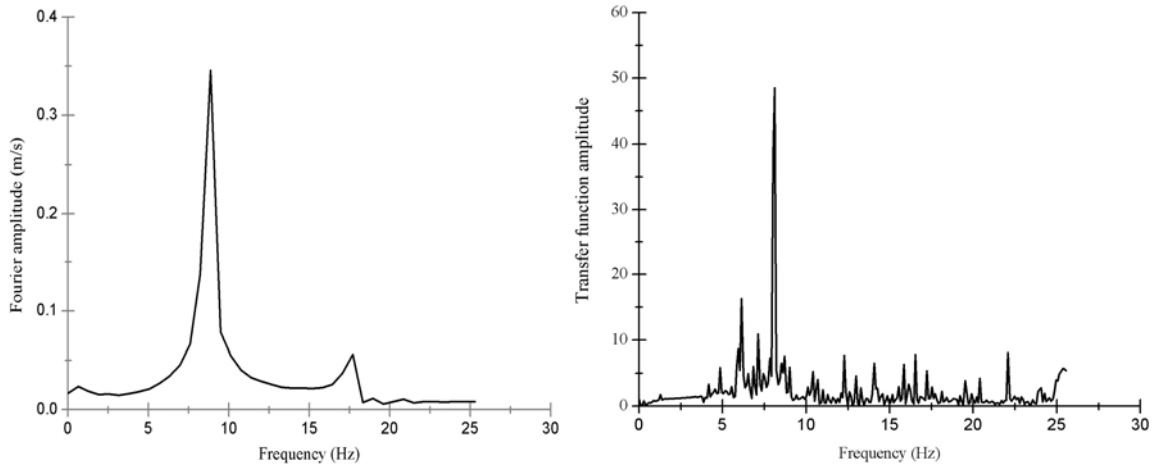

Fig.23(a). Fourier transform of the free vibration response and (b) Transfer function of the dry sand found experimentally.

From (Fig.23(a)) it may be observed that the natural frequency of the sand comes out to be around 8.64 Hz. To double check the natural frequency of the soil obtained by free vibration analysis, transfer function (i.e., the ratio of Fourier amplitudes of the top and bottom acceleration time histories) has been found out experimentally shown in (Fig.23(b)) and it is observed that the natural frequency of the soil is 8.14 Hz (corresponding to the highest peak) which is close to the value obtained by the free vibration response which validates the frequency of the soil column. The damping ratio of the sand is estimated by approximating

the free vibration response of the acceleration time history at the end of the motion as given by (Eq.2) [5]:

$$\ddot{u}(t) = Ae^{-2\pi f_n t\xi} \qquad \text{Eq.(24)}$$

where f_n is the natural frequency of the sand (=8.14 Hz) which is identified from the transfer function, ξ is the damping ratio of the sand. Therefore, approximating the decay by (Eq.24), the damping ratio of the sand is found to be around 2.27% as shown in (Fig.24),

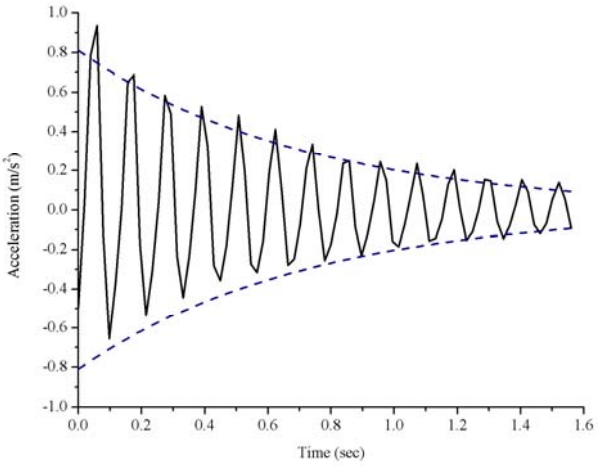

Fig.24. Free vibration response of dry sand and its exponential decay curve.

4.3. Response of Nonlinear Soil to Harmonic Waveforms

Frequency harmonics are typically generated as waves propagate in nonlinear media . As the wave propagates through the material, the wave will become distorted as the result of several sources of nonlinearity within the material . For an induced monochromatic wave excitation, the distortion of the wave results in the generation of harmonics of the main frequency. However, we hereby present an intuitive description of the generation of harmonics in terms of stress waveforms resulting from the excitation of a nonlinear soil material experimentally and numerically. The response of the soil column obtained from the bottom and top accelerometers of the test is shown in (Fig.25) along with a close up view of the asymmetric response of the soil response acceleration. Hence, it is seen from the mathematics, that if a stress/acceleration wave has half wave symmetry, one can expect odd harmonics in its fourier spectrum.

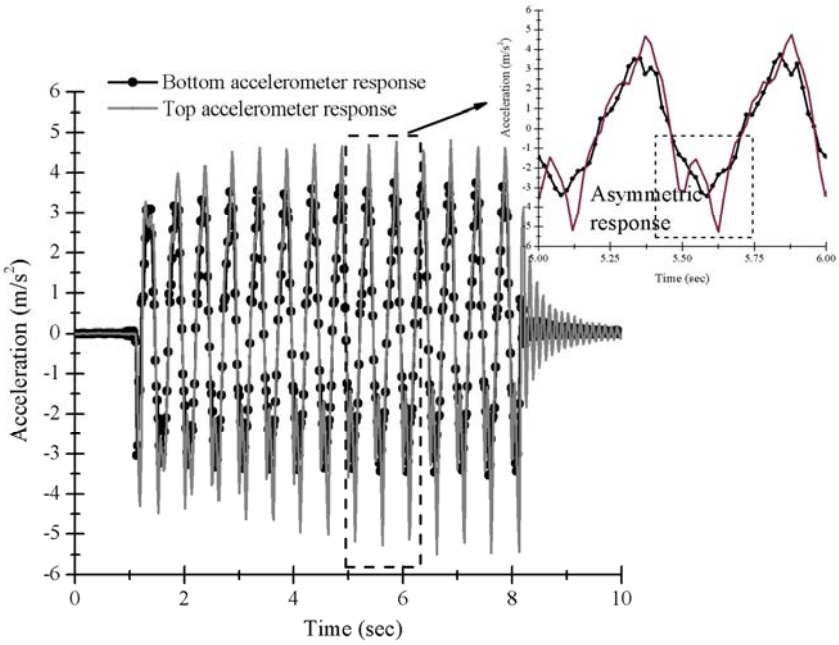

Fig.25. Acceleration time history near the top and bottom of sand bed, and the close view which shows the amplification of acceleration response.

The shear stress time history is found out from the observed acceleration record as per (Eq.25) [36],

$$\tau_i(t) = \sum_{k=1}^{i-1}(\ddot{u}_k(t) + \ddot{u}_{k+1}(t))\rho\Delta z_i/2 \qquad \text{Eq.(25)}$$

where, ρ is the density of the soil, Δz_i is the spacing interval between the two accelerometer readings.Following the above procedure, the shear stress time history for the soil is plotted in (Fig.26),

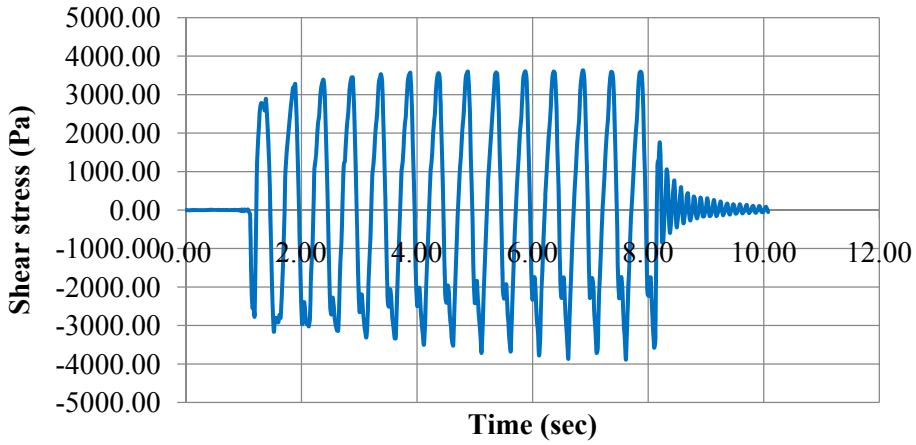

Fig.26. Time history of shear stress on the soil.

The Fourier spectrum of the shear stress time history for the same time window is plotted in (Fig.27),

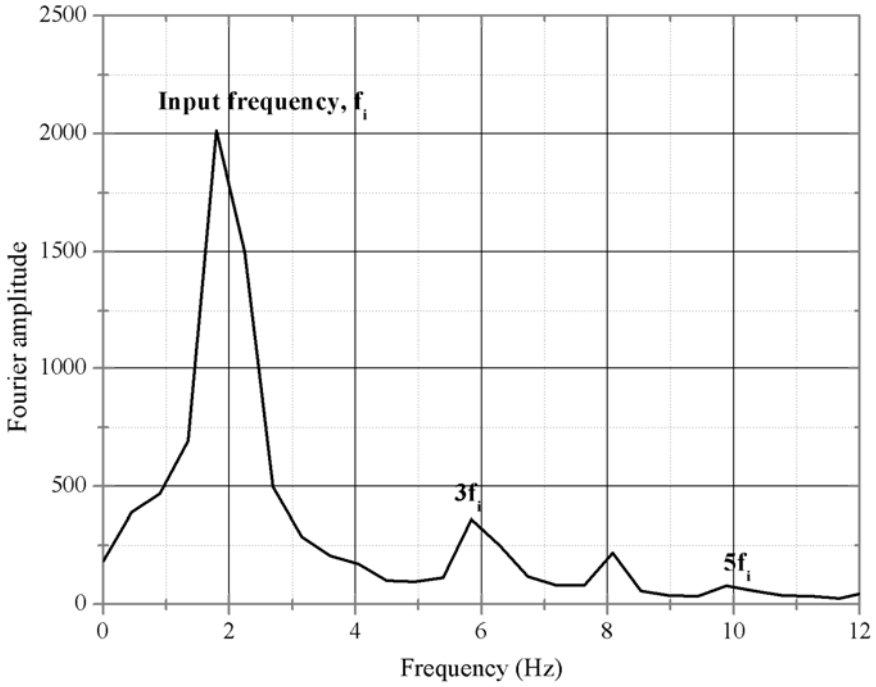

Fig.27. Fourier transform of the shear stress response for a time window of 4 to 6 secs.

From this Fourier spectrum, it is seen that there are higher harmonics generated which are odd ratios of input frequencies as expected previously. The described waveforms, which are associated to hysteretic non-linear behaviour, correspond to functions of time having half-wave symmetry: $F(t + \pi) = -F(t)$. The Fourier series of such functions contains only odd harmonics of the fundamental excitation frequency f_1 (nf_1; n = 1, 3, 5, ...) [33]. A series of numerical simulation were performed to simulate the stress response of soil materials experiencing different levels of nonlinearity. For each simulation, a sinusoidal cyclic shear strain with a certain amplitude and an excitation frequency f_1 = 2 Hz was introduced into the adopted cyclic stress-strain model as given in (Eq.11) with s=1.0 or 0.73. A single soil element of 1m in height with mass density of 1600 kg/m^3, G_{max}=20000 kPa is tested for various levels of shear strain amplitudes keeping the value of γ_{ref} as 0.1%. The unload-reload portions follow the first two Masing rules which is meant for constant amplitude of cyclic loading.

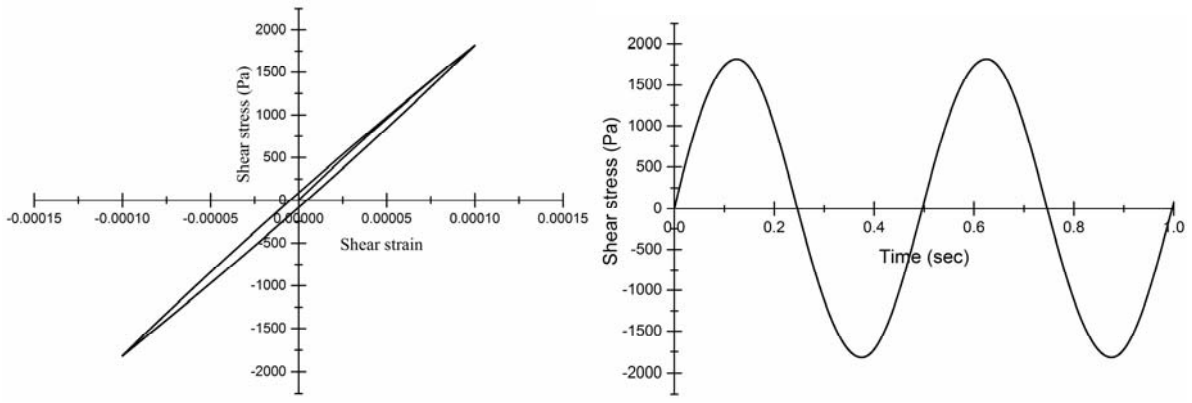

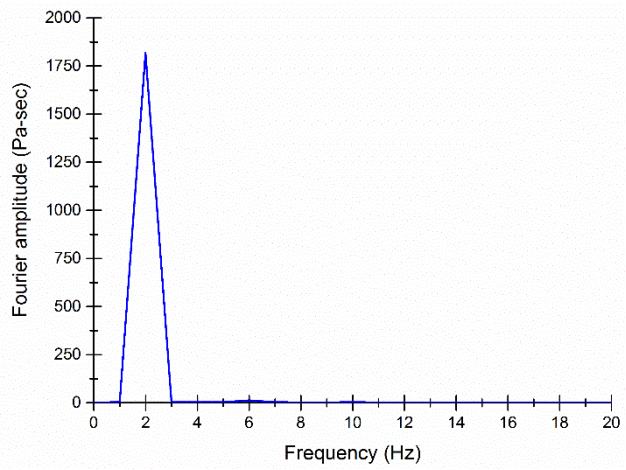
Fourier amplitude (Pa-sec)
2000
1750
1500
1250
1000
750
500
250
0
0
2
4
6
8
10
12
14
16
18
20
Frequency (Hz)

(a)

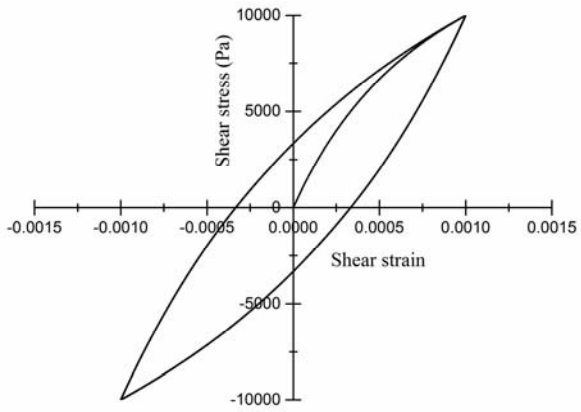
Shear stress (Pa)
10000
5000
0
-5000
-10000
-0.0015
-0.0010
-0.0005
0.0000
0.0005
0.0010
0.0015
Shear strain

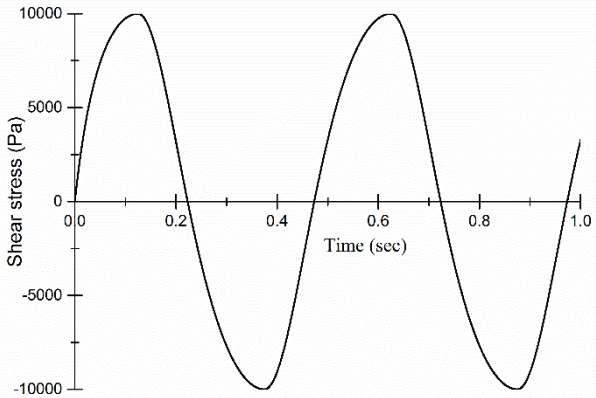
Shear stress (Pa)
10000
5000
0
-5000
-10000
0.0
0.2
0.4
0.6
0.8
1.0
Time (sec)

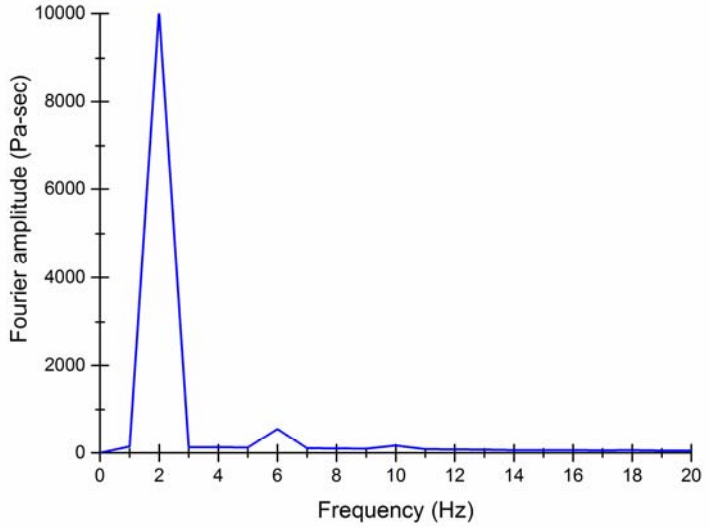
Fourier amplitude (Pa-sec)
10000
8000
6000
4000
2000
0
0
2
4
6
8
10
12
14
16
18
20
Frequency (Hz)

(b)

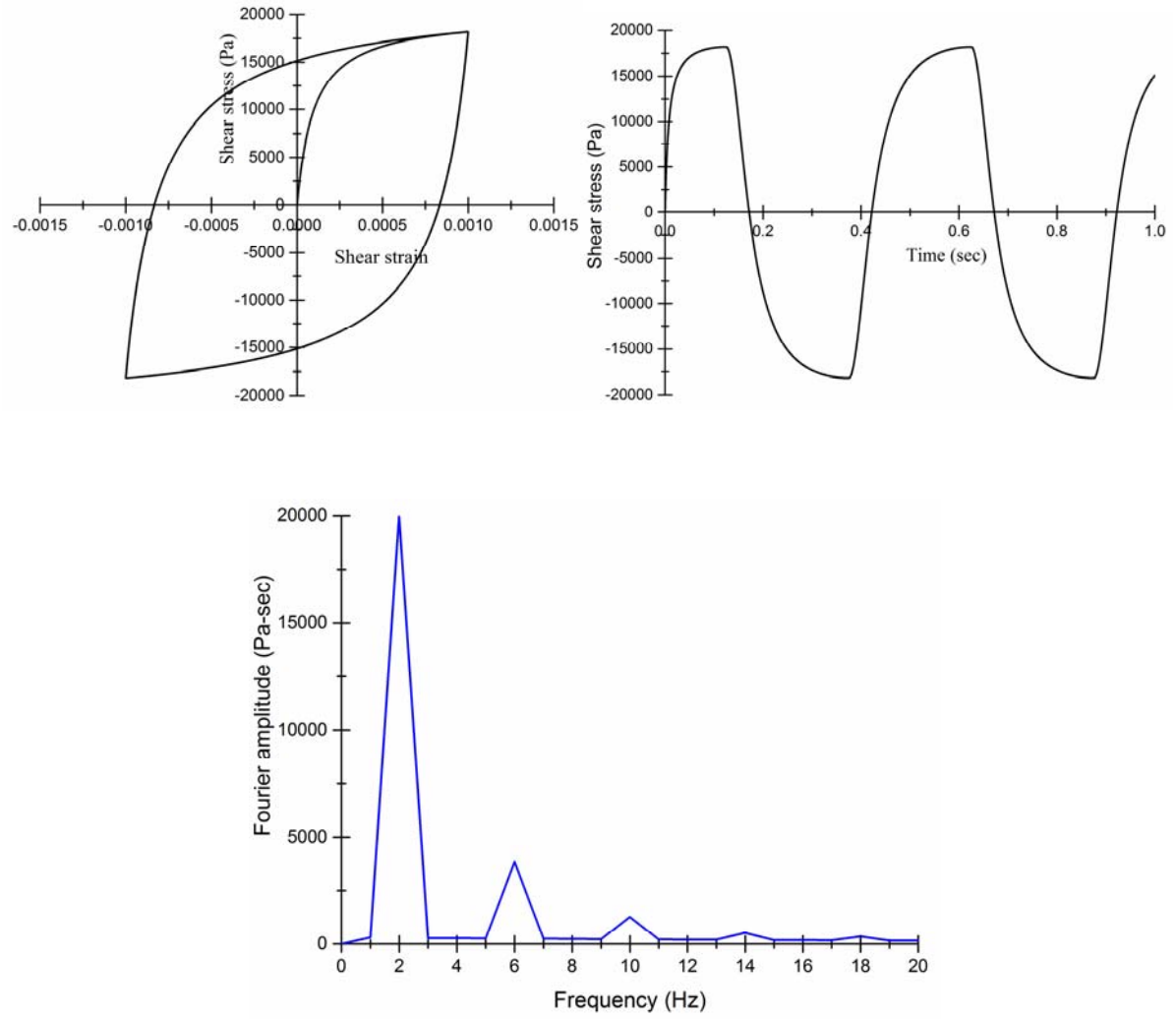

(c)

Fig.28. Shear stress-strain hysteresis and associated frequency spectra of the shear stress responses for strain amplitude of (a) 0.01%, (b) 0.1% and (c) 1%.

For a soil having a small non-linear behaviour with strain amplitude of 0.01%, the associated stress response is approximately proportional to the imposed strain (Fig.28(a)) which can be confirmed with the plot of shear stress which is approximately sinusoidal in nature. If we see the frequency spectrum of the shear stress time history, it is observed that the amplitude of the harmonics is having a very small value. As the hysteretic nonlinearity increases (due to the increase in the strain amplitude from 0.1% to 1%), the resulting shear stress time history has a "shark fin" waveform behaviour. The frequency spectrum plot has a considerable amplitude of the odd harmonics which is seen in (Fig.28(b)-(c)). Thus, it can be concluded that if the shear stress is anything other than a sine wave, high frequency harmonics of the input motion are likely to be present on the shear stress (or acceleration) responses [32]. This study also proves the explanation of the existence of high frequency content (or multifrequency output).

5. ANALYSIS AND NUMERICAL SIMULATION (1-D) FOR HIGH STRAIN TEST: EFFECT OF STRAIN DEPENDANT DAMPING RATIO IN THE RESPONSE OF SOIL COLUMN

The numerical algorithm created are validated with the experimental results conducted at high strains using the same lumped mass formulation as described previously, except that there is a slight modification (s<0, > 0, but not equal to 1.0) in (Eq.11) in the backbone curve to match the damping ratio at high strains which is an essential parameter to be calibrated for validating the results at larger strains. The numerical discretization is shown in (Fig.29) below,

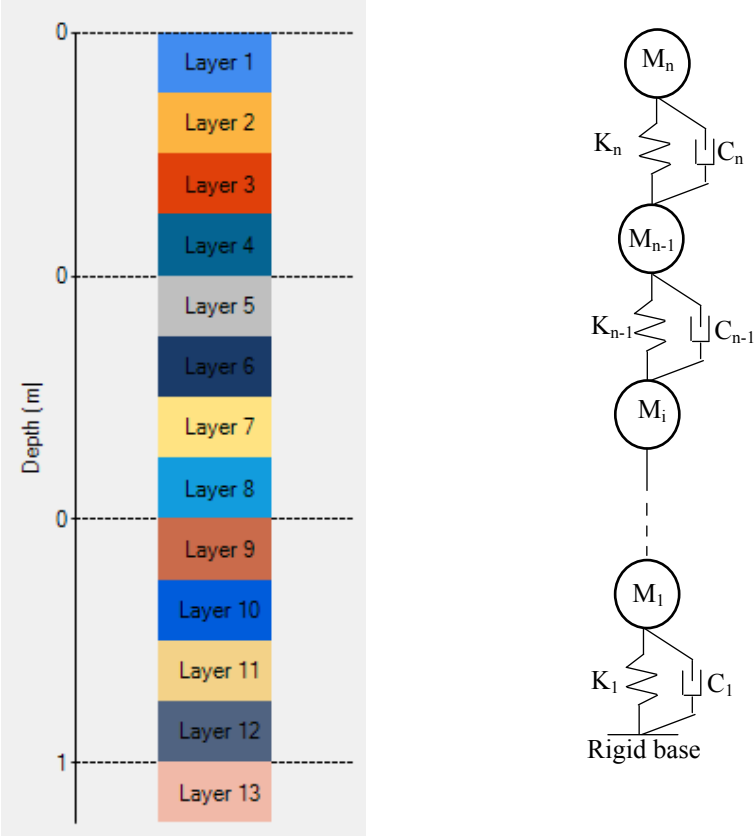

Fig.29. Numerical discretization of soil column in a shake table test.

The element size is chosen to be 0.05 m with due regards to the maximum frequency that an element can propagate (after [16]). It is assumed that the cyclic soil behaviour used for modelling the nonlinearity and the shake down of the strength of the foundation dry Kasai River sand during the dynamic loading conditions follows the relationship shown in (Fig.30),

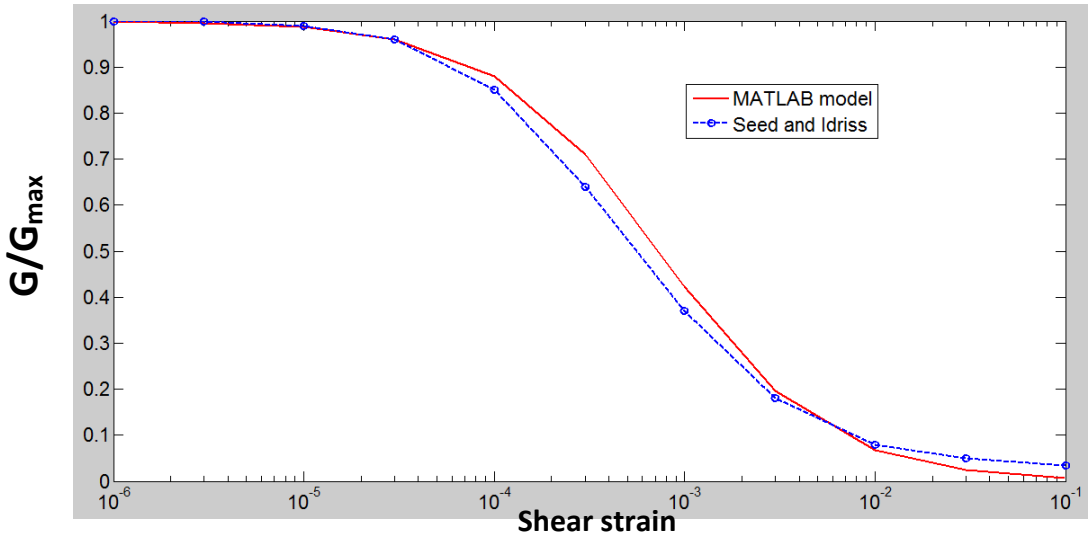

(a)

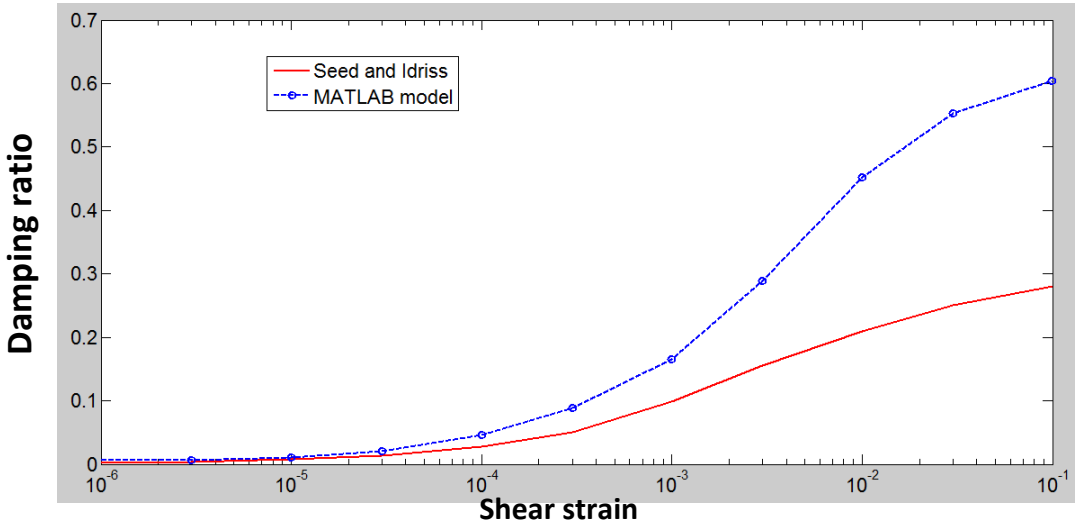

(b)

Fig.30. Calibration of the (a) shake down strength and (b) damping ratio dependency of sand with shear strain.

For low to medium strains, the hyperbolic model is good to predict the responses, but for higher strains there is a significant difference in the damping values which is seen from the plots of calibration program, (γ_{ref}=0.00074 used for the match). Due to high strain mismatch in the damping ratio based on Masing rules leads to an underestimation of shear strains and/or surface intensities at the ground surface [23] which is also observed in the developed model below (With 1% small strain damping) as is seen in (Fig.31),

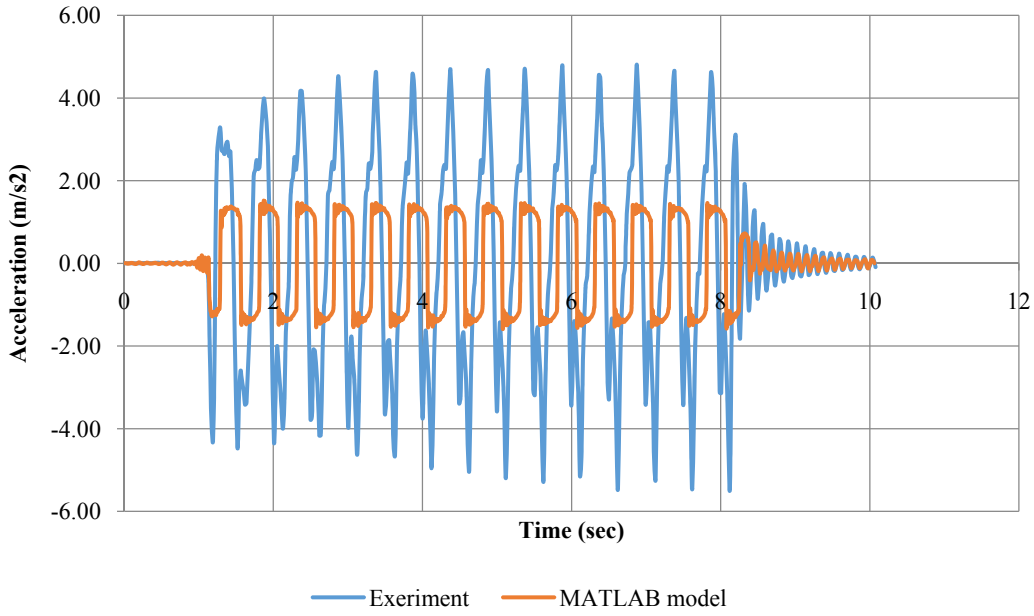

Fig.31. Experiment and numerical comparison of acceleration time history near the top surface of sand.

This mismatch is expected because of the mismatch in the damping ratio at higher strain levels. This can be fixed if there is a way to calibrate in such a way that there is a reasonable fit of shear modulus degradation and damping ratio for the entire strain range. Hence, for high strains, the value of 's' (refer to (Eq.11)) is not equals 1 to match the damping ratio curves with a mismatch for the modulus reduction curves as shown in (Fig.32),

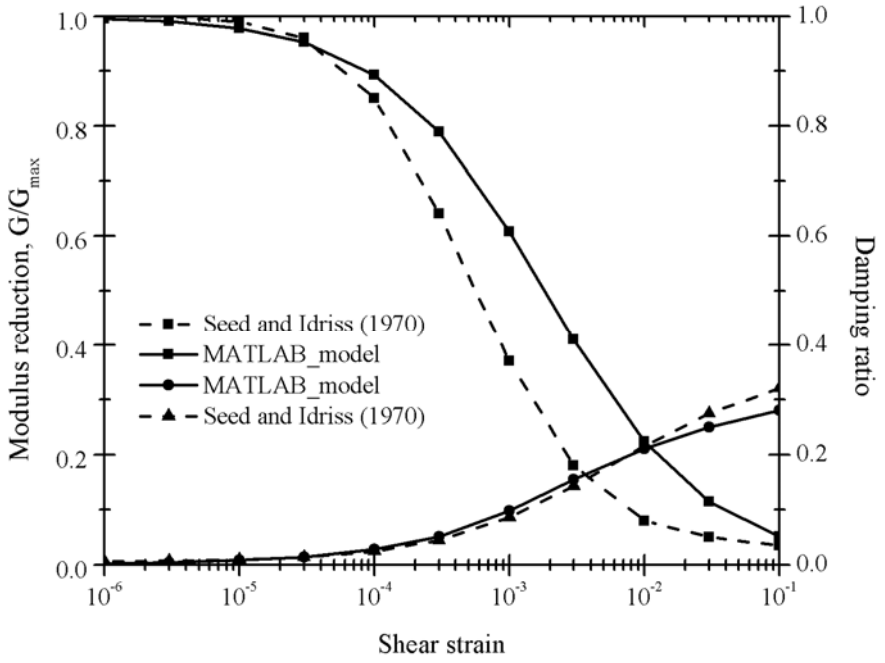

Fig.32. Modified calibration of the shake down strength and damping ratio dependency of sand with shear strain.

In this curve, the curve fit parameters (refer to (Eq.11)) are γ_{ref}=0.0088, s=0.73 are used for the match. The calibration code is attached in the Appendix. Thus, there is a reasonable match with the damping ratio curve for higher strains. Using this model, the response acceleration at the top and the bottom surface of sand is plotted in (Fig.33) below,

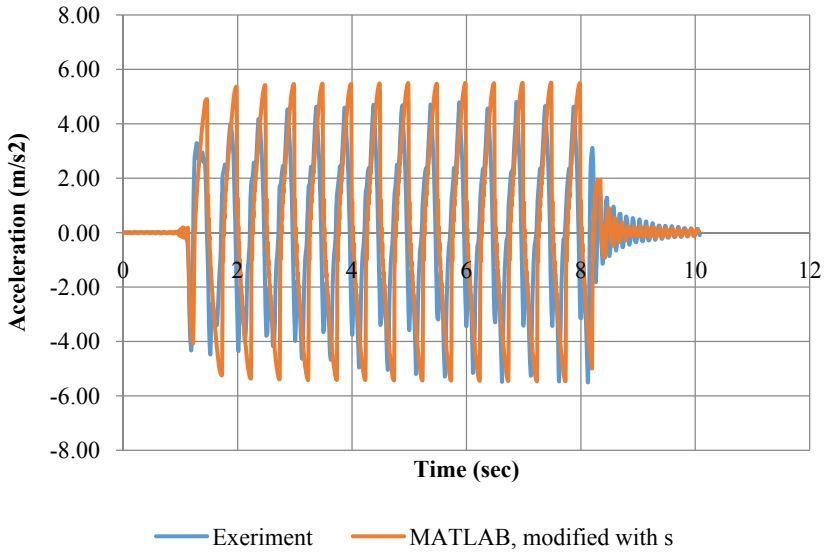

Fig.33. Experiment and numerical comparison of acceleration time history near the top surface of sand.

It is seen that there is a drastic improvement in the results of acceleration time history obtained by modifying the backbone curve. Improved match for damping ratio curve has led to improvement in the acceleration prediction from the developed model (with 1% small strain damping). The shear strains are on the order of more than 8%. For illustration, a sample shear stress-strain loop at a depth of 0.4m from the top surface of soil is shown in (Fig.34) below,

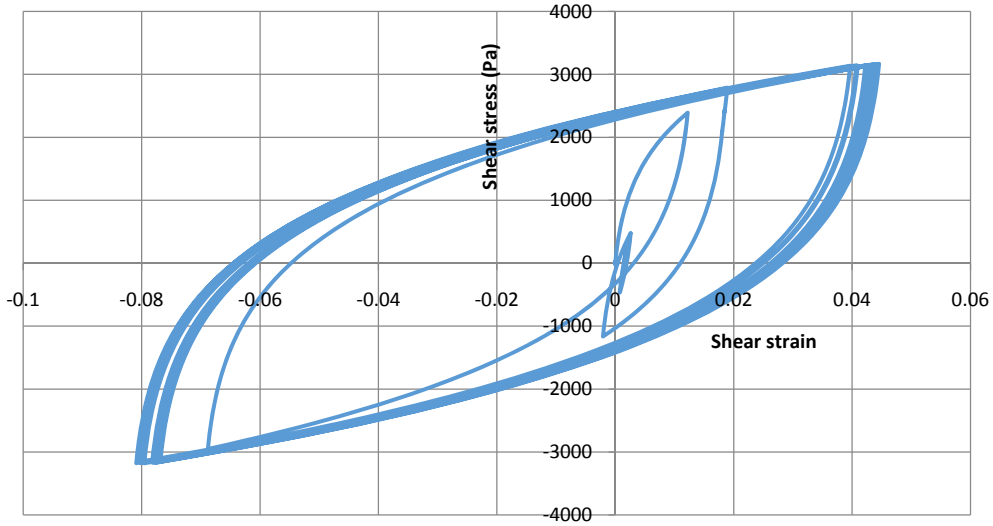

Fig.34. Stress-strain hysteresis loops of sand at a depth of 0.4m from the top surface.

It is to be noted that the mismatch in the acceleration seen in (Fig.31) is also because the experiment is not vertically propagating shear waves. This is an important limitation. In the simplified lumped mass approach, it is simulating exactly vertically propagating shear wave which is not the actual case. Hence, the numerical model is not representative of the experimental model because the boundary conditions are not simulated as in the experiment. Hence the results obtained from this model cannot be relied upon since we are not simulating the exact wave nature of wave propagation in a rigid tank. The match may be good from this model in this case which maybe due to less boundary effects in the recorded acceleration time history, but this might not work well for other cases. This exercise is done only to illustrate the importance of matching the strain dependant damping ratio of soil and what effect it can have on the behavior of intensities near the ground surface. For representing the exact boundary condition of this experiment, a full nonlinear 2D or 3D model is required to be performed with free field boundary conditions at the sides of the soil column [2] and [9] which has been done in the forthcoming section.

6. INFLUENCE OF THE MULTILINEAR NATURE OF THE BACKBONE CURVE ON THE NONLINEAR SOIL RESPONSE

A series of numerical simulation were performed to simulate the shear stress response of soil material with two types of backbone curves namely hyperbolic [34] and multilinear [13 & 14] model (based on distributed elements). A single soil element of 1m in height is subjected to a cyclic shear strain (or displacement) of amplitude 5% with an excitation frequency f_i = 2.0 Hz (chosen arbitrarily). The soil column is fixed at the base and the shear strain is applied on the top of the soil column which nullifies the inertial effect of the soil and the problem reduces to a simple shear test. As the applied strain is of constant amplitude, hence the unload-reload portions follow the first two Masing rules [18]. In the hyperbolic model, the equation of a backbone curve which has gradual stiffness transition is utilized is shown in (eq.11). As the numerical study is conducted at higher strains, if there is a mismatch between the damping ratio at higher strains, then it leads to an under-prediction of the intensities near the surface such as the free surface acceleration as well as the maximum shear stress experienced by the soil [23] which is also seen from (Fig.30). Hence, the calibration is done for the damping ratio curve which leads to a mismatch for the modulus reduction (or the shake down strength) of the soil as seen in (Fig.31). For running the simulation, the hyperbolic backbone curve parameters are calibrated such that it complies with the damping ratio curve proposed by [27]. An in-house code has been developed following a modified hyperbolic backbone curve as shown in (Eq.11) for calibration of the modulus reduction and damping ratio curves, following the procedure of [29]. For a reasonable match for the damping ratio curves which in turn leads to a mismatch for the modulus reduction, the value of γ_{ref} and s is found to be 0.0088 and 0.73 respectively. The corresponding curves are shown in (Fig.31). Using this backbone curve parameters, the multilinear backbone curve is fitted up to a shear strain amplitude of 5.0% with varying number of parallel springs namely 4 and 9. The procedure of fitting the multilinear backbone curve is proposed by [14] and an in-house program has been developed for the same. This procedure is based on overlay modelling concept in which N number of parallel elastoplastic springs are operating in tandem. The parallel spring elements are having equal displacements (or strains), hence the total stress of each springs is added to

get the final stress corresponding to the applied strain. This multilinear model represents Bauschinger effect and extended Masing behaviour in a straightforward manner [14]. The total shear stress for a given shear strain γ is represented by the sum of elastic and plastic components as shown in (Eq.26):

$$\tau = \sum_{j=1}^{n} G_j \gamma + \sum_{j=n+1}^{N} \tau_{yj} \quad \text{Eq.(26)}$$

, in which n is the number of springs which are in elastic state and the rest have already gone into plastic state with yield strength τ_Y. The procedure of obtaining the individual shear modulus (G_j) of each spring is already described in detail in the methodology proposed by [14] and hence is not elaborated in this study. Following the above methodology, a fit of multilinear curve with hyperbolic (continuous) stress strain curve with 4 number of parallel springs is shown in (Fig.35).

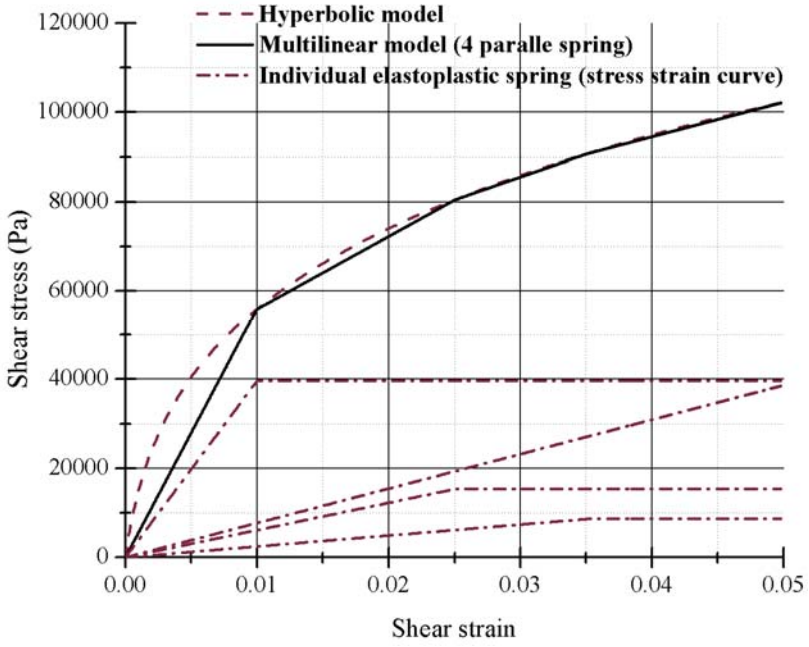

Fig.35. A fit of multilinear curve with hyperbolic (continuous) stress strain curve with 4 number of parallel springs.

To understand the effect of the sharp change in slope in the high frequency harmonics, two types of backbone curve was selected namely hyperbolic and multilinear (with distributed elements 4 and 9 in numbers). The soil element was subjected to shear strain in each of the models and its corresponding stress-strain loops are plotted in (Fig.36).

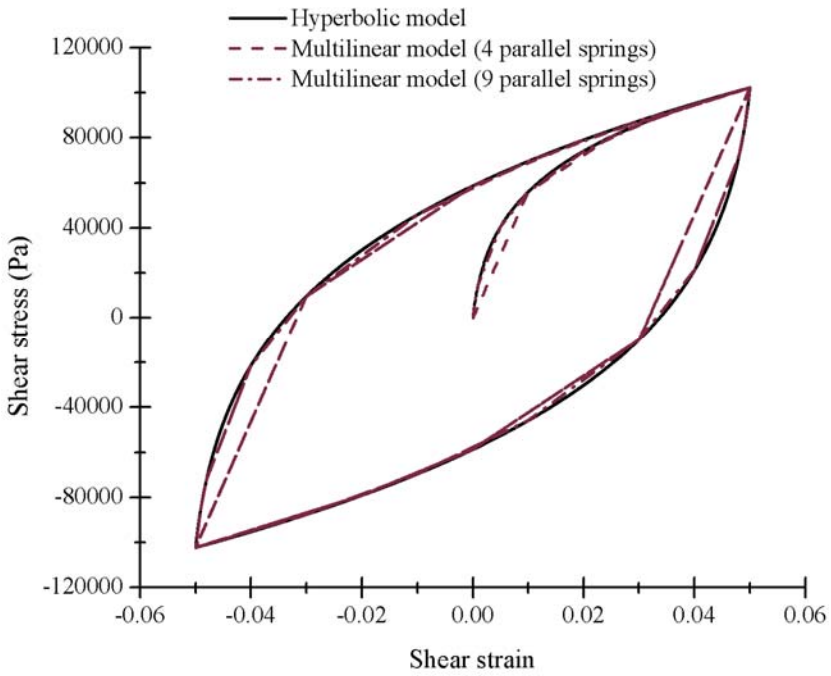

Fig.36. Shear stress strain loops obtained from the hyperbolic, multilinear (4 points) and multilinear (9 points) model.

The shear stress time history for the hyperbolic model is also plotted in (Fig.37) which shows asymmetricity in the peaks (deviation from pure sinusoid) which is caused due to pointed nature of the hysteresis loops at the ends.

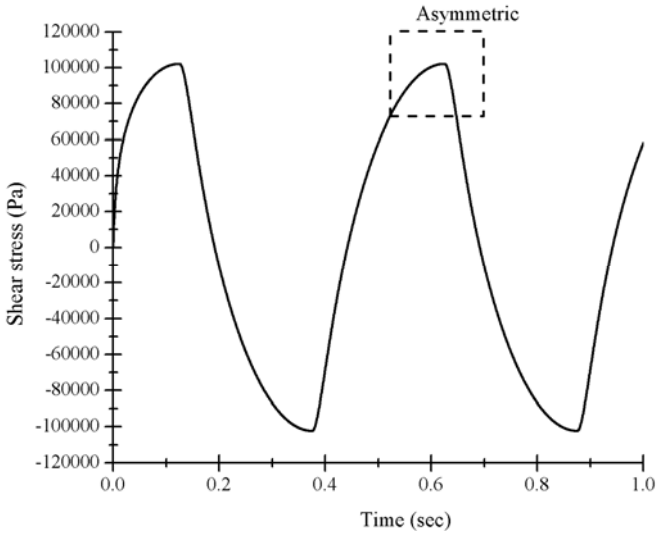

Fig.37. Shear stress time history obtained from the hyperbolic model.

The Fourier spectrum of the shear stress time histories obtained from the hyperbolic and multilinear models are plotted in (Fig.38) in which a closer look reveals that the predominant frequency is 2.0 Hz which is the input frequency. In addition, there are other harmonics which are odd multiples of the input frequency in which peaks are observed namely at 6 Hz, 10 Hz etc., which continues till infinity. The observed phenomena is termed as Gibbs

phenomena [8], in which an infinite sum of harmonic (sine or cosine) waves are required to represent a piecewise differentiable waveform (i.e., waveforms with asymmetricity).

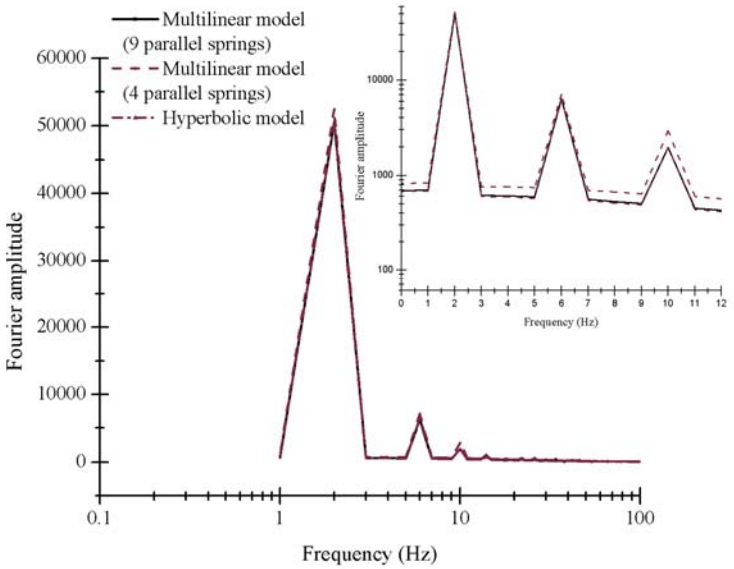

Fig.38. Fourier spectrum of the shear stress time history obtained from the hyperbolic and multilinear model.

Another thing is to be noted that there is a sharp change in the slope during the loading process for multilinear loops which is one of the cause for the increase in the amplitude of the already existing high frequency harmonics. As the number of parallel springs are increased, the slope changes become gradual during loading and the amplitude of the high frequency harmonics comes close to the values predicted by hyperbolic model. In addition to these, during the loading/unloading it is seen that the introduction of sharp points in the hysteresis loops corresponds to a sudden change in the stiffness of the soil which was identified by [35] and is one of the reason for the higher frequencies in a nonlinear analysis. Thus, these results provide a reasonable explanation to the origin of the high frequency (odd) harmonics in the frequency content of the response histories both experimentally as well as numerically. It is also clear that the high frequency content is also related to the shape of the hysteresis loops as identified by [32]. From the experimental observation, presence of asymmetricity in the top acceleration response history confirms that the stress-strain loops are not rounded at the edges hence there is a subtle reason to believe that the loops might be pointed at the edges which might be a reason for the origin of the high frequency harmonics, although there are **no concrete experimental evidence** for the actual nature of the hysteresis loops.

7. SIMULATION OF HIGH STRAIN TEST BY 2-D PLANE STRAIN ANALYSIS

The sand bed in the foundation (1.00 m in width and 0.65 m in height for dry sand) is discretized by 20 x 13 numbers of quadrilateral elements of sizes 0.05 m×0.05 m. The locations of the side and the bottom boundaries in the numerical analyses are chosen to satisfy the dimensions of the sand bed in the shake table model tests. The plexiglass test chamber, within which the laboratory model tests are conducted, is not modelled in the

numerical analyses. In the static analysis, the soil-structure system is under gravity loading only. The bottom boundary is fixed in all directions and the side boundaries are fixed in the horizontal (x) direction only. It may be noted that during the static analysis, the flow calculation option in the program is turned off, as no water is involved in these tests and the sand is in dry condition. After performing the initial static analysis, the dynamic analysis is performed. In the dynamic modelling, the wave propagation through the soil (media) is of considerable importance. The finite difference grid dimensions are selected by considering the maximum frequency (*f*) of the shear wave that the model could logically respond during earthquake loadings. The element size is chosen to be 0.05 m with due regards to the maximum frequency that an element can propagate (after [16]). As the experiment is conducted on a tank with rigid walls, the shear waves are not vertically propagating hence there may be considerable reflection from the boundaries although there are 32 mm thermocols present. This boundary condition is simulated by applying free field on the sides of the soil domain. It is not recommended to use pure shear boundaries at the sides of the soil column because of the behaviour of the soil is not similar to that inside the laminar box. The lateral boundaries of the main grid are coupled to the free-field grid by viscous dashpots to simulate a quiet boundary (see (Fig.39)), and the unbalanced forces from the free-field grid are applied to the main-grid boundary. The free-field model consists of a one-dimensional "column" of unit width, simulating the behavior of the extended medium. The acceleration-time histories (Fig.21) as applied to the shake table model tests, is assumed to be acting at the bottom of the soil domain. The numerical model (with the discretization) along with the boundary conditions are shown in (Fig.39). The soil behavior under the dynamic loading is described by a nonlinear hysteretic behaviour available in the finite difference program. It is assumed that the cyclic soil behavior used for modelling the nonlinearity and the shake down of the strength of the foundation dry Kasai River sand during the dynamic loading conditions follows the relationship proposed by [27], Upper Range. This curve is used as an input of the hysteretic behavior ("*sigmoidal*" model) in the numerical simulation. The "*sigmoidal"* curves are monotonic within the defined range, and have the appropriate asymptotic behaviour. Hence these functions are well suited for representing modulus degradation curves. The "*sigmoidal"* model in the finite difference program (namely, *sig3*) is defined as follows:

$$M_s = \frac{a}{1+\exp\left(\frac{-(L-x_o)}{b}\right)} \qquad \text{Eq.(27)}$$

Where, L is the logarithmic strain, $L = \log_0(\gamma)$, a, b and x_o are the curve fitting parameters whose values are 1.0, -0.5692 and -0.854, respectively for the curve shown in (Fig.32). In the numerical computation at each calculation step, the hysteretic model is used to update the tangent shear modulus (M_t) of the nonlinear soil model. To suppress the high frequency noise in the obtained acceleration time history, 3.00% viscous damping with minimum frequency (f_{min}) of 3.162 Hz has been added in addition to the hysteretic damping of the soil.

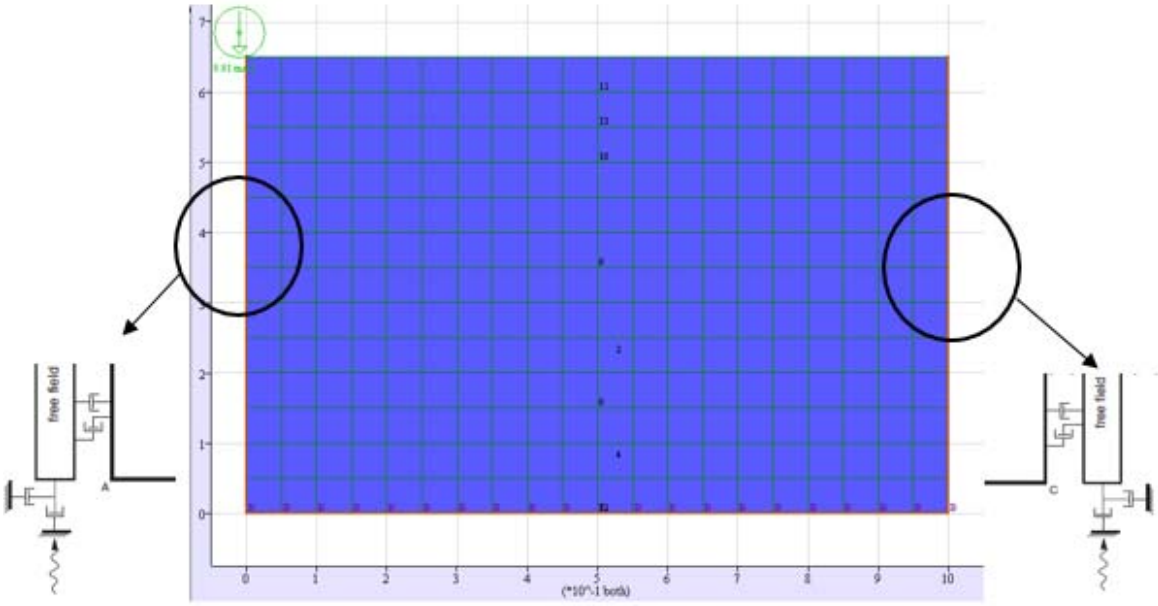

Fig.39. The numerical model (with the discretization) along with the boundary conditions.

7.1. Results of Numerical Simulation

The results of the numerical analysis are compared with the results of the corresponding shake table model tests as seen in (Fig.40(a&b)). The frequency content of the experiment and the numerical prediction is compared for a time window of 4.0-7.0 secs which is also shown in the figures.

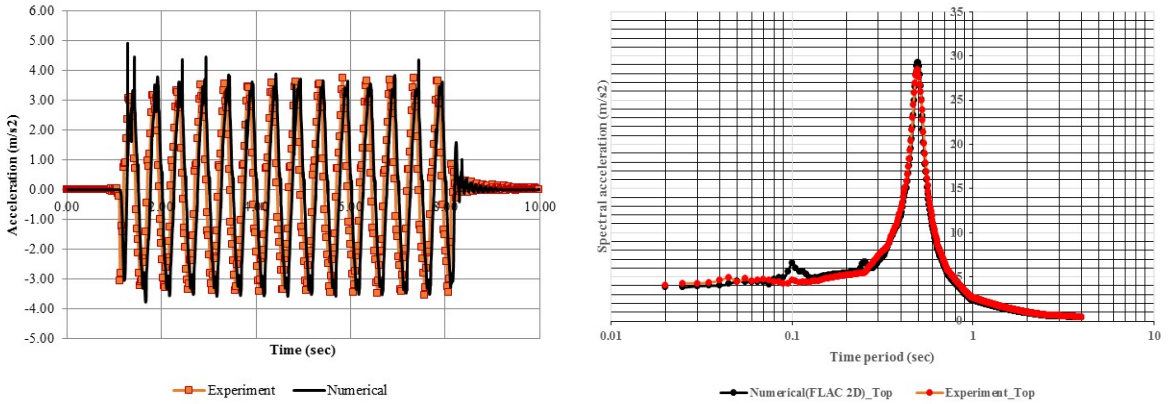

(a)

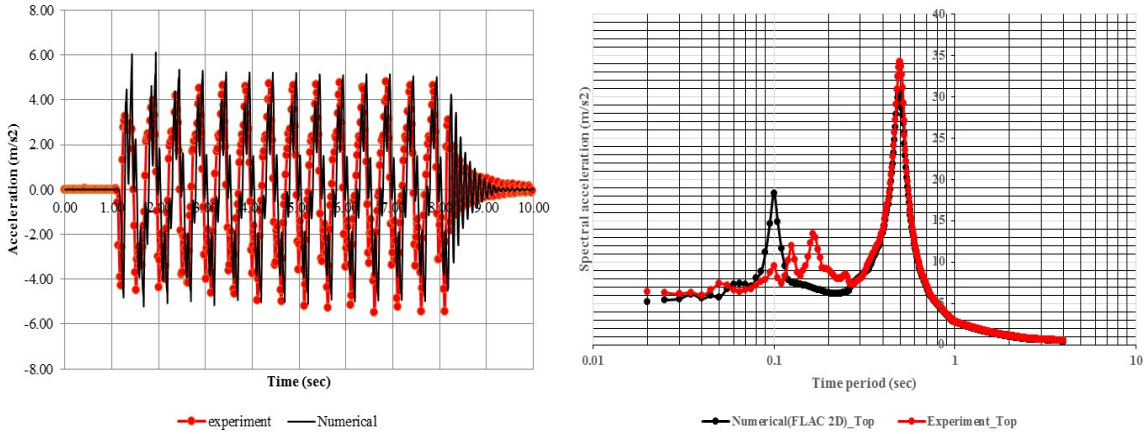

(b)

Fig. 40(a)-(b). Acceleration time histories obatined from experiment and numerical analysis for bottom and top soil for dry sand test.

It is seen from the results that the time histories for the acceleration match well for nonlinear hysteretic model both in top and bottom location of the sand. A shear stress-strain loop at a depth of 0.55m from the top of the sand layer is obtained numerically which is shown in (Fig.41) and it is seen that the shear strain experienced by the soil is beyond 3%.

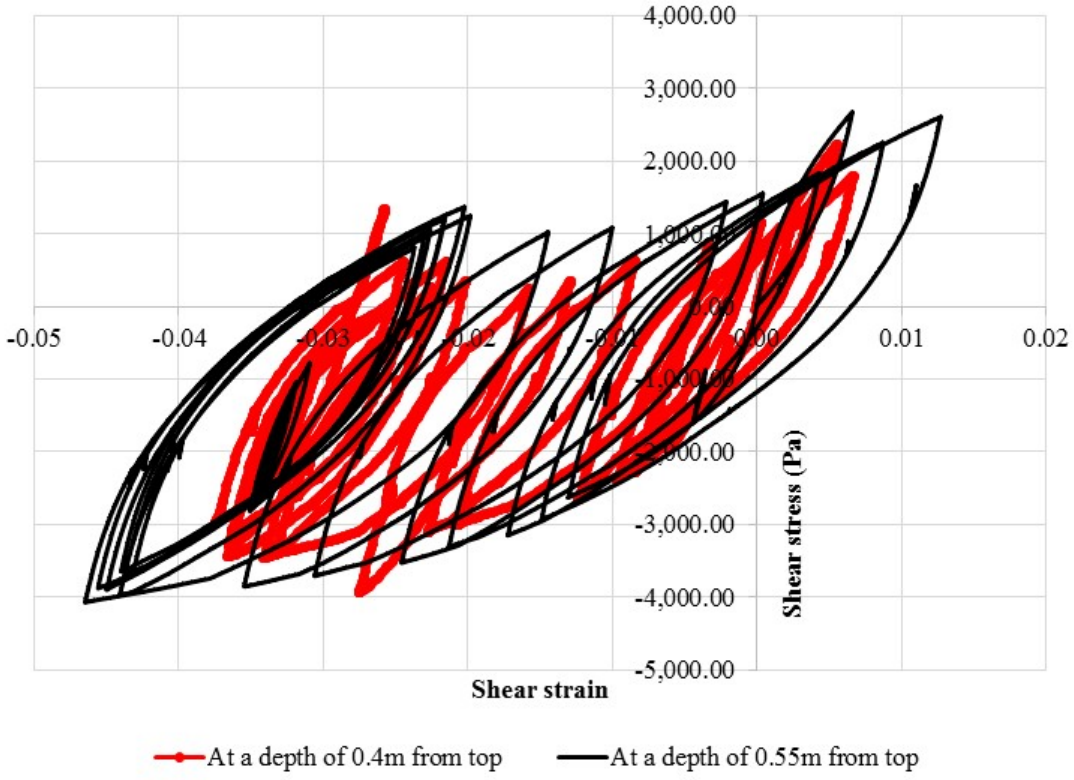

Fig.41. Hysteresis loops obtained from nonlinear model at a depth of 0.4m & 0.55m from the top of sand layer.

The entire study has been conducted based on the actual strain dependant strength (G/G_{max}) of the soil where there is an *"implied shear strength of the sand"* (based on the static soil properties measured at shear strains well above 1.0%) which does not change with the function of confining pressure. This impled shear strength may or maynot be realsitic, thus potentially underestimating or overestimating the actual strength depending on the depth. This happens because the G/G_{max} curves are simply extrapolated to more than 1.0% shear strain following a hyperbolic trend without consideration for the shear strength impled by the large strain portion of the curve. This problem is to be addressed in the future studies by modifying the target G/G_{max} curve manually or by nonlinear curve fitting procedure beyond shear strains greater than 0.1% so that the shear stresses better approximate the target static shear strength at a shear strain range of 3.0-5.0%.

8. CONCLUSIONS

The purpose of this study is to understand the behaviour of the structures resting on soil layers above the bedrock. Hence, seismic ground response analysis is required to develop the site-specific response spectrum for the design of important superstructures in the region. Site response analysis is performed in both equivalent linear and nonlinear time domains. In this study, both equivalent linear and nonlinear ground response analyses have been utilised for validating the experiments conducted on F-55 Ottawa Sand in GLB conducted at the University at Buffalo, State University of New York. The observation of this study is that the nonlinear time domain analysis is more time consuming than the equivalent linear analysis, but in terms of prediction of the results, nonlinear analysis is better than the equivalent linear analysis (because of its inherent limitations [11] and hence, this methodology is preferred. For validating the developed nonlinear model at higher stains, shake table test was conducted at IIT Kharagpur and it was found that a slight modification in terms of introduction of a power 's' (nonzero) (refer in (Eq.11)) is required to validate the model at higher strains. This study also addresses the issues for the generation of high frequency harmonics other than the input motion in a nonlinear analysis of soil. The high frequency harmonics are observed experimentally in the free surface acceleration/shear stress in a shake table test conducted for large strain on a dry Kasai river sand subjected to a sinusoidal excitation of 0.35g with a frequency of 2 Hz. It is observed that the harmonics of the input frequencies are observed on the frequency spectrum of the time histories of acceleration/shear stresses. This observation is supported by numerical explanation by conducting a nonlinear site response analysis of a single soil element using hyperbolic and multilinear stress strain models, which is subjected to a harmonic shear strain (or displacement) of a single frequency which is used to study the frequency content of the response histories in terms of free surface acceleration, stresses etc. It is also observed that the amplitude of harmonics is dependent on the number of parallel springs chosen for generating the multilinear stress strain curve. In addition, the results of the dynamic model tests are compared with the results from a plane strain finite difference program in terms of acceleration time history at the top and bottom accelerometer locations and it is found out that the numerical predictions are in reasonable agreement with the experimental observation using hyperbolic nonlinear stress-strain soil model. Although the numerical predictions are well in agreement with the experimental datas, but shear strength correction for strain dependant G/G_{max} must be

performed before conducting any site response analysis study so that the soil doesnot experience unrealistic shear strength at any depth under large strains (>0.1%).

ACKNOWLEDGEMENT

While bringing out this report to its final form, we came across several people whose contribution in various ways helped our understanding. It is a pleasure to convey our gratitude to the Facility Risk Group at Idaho National Laboratory for sharing their experimental results and for providing various help during this study. The first author also acknowledges that the high strain tests were performed at the shake table facility at the Geotechnical laboratory of IIT Kharagpur which is provided by SERB, DST, New Delhi vide a grant no. SR/S3/MERC-0029/2011.

REFERENCES

[1] Abel, J and Shephard, M.S. "*An algorithm for multipoint constraints in finite element analysis",* International Journal for Numerical Methods in Engineering, 14(3):464 – 467, 1979.

[2] Banerjee, R. et al. "*Shake Table Tests and Numerical Modeling of Kasai River Sand,"* Geotechnical and Geological Engineering, 35(4):1327-1340, 2017.

[3] Bhattacharya, S. et al. "*Model Container Design for Soil-Structure Interaction Studies",* In: Role of Seismic Testing Facilities in Performance Based Earthquake Engineering, v.2, edited by Michael N. Fardis and Zoran T. Rakicevic, (Series: Geotechnical, Geological and Earthquake Engineering), Netherlands: Springer, 135-158, 2012.

[4] Chopra, A.K. *"Dynamics of structures: Theory and application to earthquake engineering",* 3rd Ed., Noida: Englewood Cliffs (India), 2007.

[5] Clough, R.W. *"Dynamics of Structures",* 2nd Ed., Singapore: McGraw-Hill, 1993.

[6] Cook, R. et al. *"Concepts and Applications of finite element analysis",* 4th Ed., New York: John Wiley and Sons, 1989.

[7] Coleman, J.L. Bolisetti, C. and Whittaker, A.S. *"Time-domain soil-structure interaction analysis of nuclear facilities",* Nuclear Engineering and Design, 298:264-270, 2016.

[8] Gibbs, J.W. *"Fourier's series,"* letter in Nature, 59(1522), 1898. Letter dated November 29, 1898.

[9] Giri, Debabrata and Sengupta, Aniruddha *"A Dynamic behavior of small-scale model of nailed steep slopes",* Geomechanics and Geoengineering: An international journal, 5(2): 99-108, 2010.

[10] Hashash, Y.M.A. and Park, D. *"Viscous damping formulation and high frequency motion propagation in non-linear site response analysis",* Soil Dynamics and Earthquake Engineering, 22(7):611–624, 2002.

[11] Hashash, Y.M.A. et al. *"DEEPSOIL 5.1, User Manual and Tutorial",* 2012.

[12] *"User's guide for FLAC version 5.0.",* Nagpur, India: Itasca India Consulting, 2005.

[13] Iwan, W.D. *"On a class of models for the yielding behavior of continuous and composite systems",* Journal of Applied Mechanics, 34(3):612–617, 1967.

[14] Kaklamanos, J., Dorfmann, L. and Baise, L.G. *"A Simple Approach to Site-Response Modeling: The Overlay Concept",* Seismological Research Letters, 86(2A):413-423, 2015.

[15] Kramer, S.L. *"Geotechnical earthquake engineering",* New Jersey: Prentice hall, 2005.

[16] Kuhlemeyer, R.L. and Lysmer, J. *"Finite Element Method Accuracy for Wave Propagation Problems",* Journal of the Soil Mechanics and Foundations Division, 99(5):421-427, 1973.

[17] Lombardi, D. and Bhattacharya, S. *"Shaking table tests on rigid soil container with absorbing boundaries",* In: Proceedings of the 15th World Conference on Earthquake Engineering, (Lisbon, Portugal: 15th World Conference on Earthquake Engineering, September 24-28, 2012), 2012.

[18] Masing, G. *"Eigenspannungeu und verfertigung beim Messing(C)",* Proceedings of the 2nd International Congress on Applied Mechanics, Zurich, 1926. (Zurich, Switzerland: 2nd International Congress for Applied Mechanics, September 12-17, 1926), page?, 1926.

[19] Mondal, J.K. and Kumar, A. *"Impact of Higher Frequency Content of Input Motion Upon Equivalent Linear Site Response Analysis for the Study Area of Delhi",* Geotechnical and Geological Engineering, 35(3):959–981, 2017.

[20] Newmark, N.M. *"A Method of Computation for Structural Dynamics",* Journal of the Engineering Mechanics Division, 85(3):67-94,1959.

[21] Newmark, N.M. "*Effects of earthquakes on dams and embankments*", Geotechnique, 15(2):139–160, 1965.

[22] NEES, Ottawa F55 Sand.https://nees.org/warehouse/specimen/project/122/experiment/4791,2009.

[23] Phillips, C. and Hashash, Y. M. *"Damping formulation for nonlinear 1D site response analyses",* Soil Dynamics and Earthquake Engineering, 29(7):1143–1158, 2009.

[24] Pyke, Robert M. *"Nonlinear soil models for irregular cyclic loadings",* Journal of the Geotechnical Engineering Division, 105(6):715-726, 1979.

[25] Rayleigh, J.W.S. and Lindsay, R.B. *"The theory of sound,"* New York: Dover Publications, 1945.

[26] Schnabel, P.B., Lysmer, J. and Seed, H.B. *"SHAKE—A computer program for earthquake response analysis of horizontally layered sites",* EERC 72-12, Earthquake Engineering Research Center, 1972.

[27] Seed, H.B. and Idriss, I.M. *"Soil Moduli and Damping Factors for Dynamic Response Analyses",* EERC 70-10, Earthquake Engineering Research Center, 1970.

[28] Spears, B. *"NLSSI High Frequency Response Study",* INL/MIS-16-39106, Idaho National Laboratory, 2016.

[29] Spears, R. and Coleman, J. *"Calibrating Nonlinear Soil Material Properties For Seismic Analysis Using Soil Material Properties Intended For Linear Analysis",* In: The 23rd International Conference on Structural Mechanics in Reactor Technology (Manchester, United Kingdom: SMIRT23, August 10-14, 2015.), Manchester: IASMiRT, Division III, Paper ID 395, 2015.

[30] Thevanayagam, S. Shenthan, T. and Kanagalingam, T. *"Role of intergranular contacts on mechanisms causing liquefaction & slope failures in silty sands",* New York: Buffalo State University ,Department of Civil, Structural, and Environmental Engineering, 2003.

[31] Vucetic M. *"Normalized behavior of clay under irregular cyclic loading",* Canadian Geotechnical Journal, 27(1):29–46, 1990.

[32] Veeraraghavan, S., Spears, R.E. and Coleman, J.L. *"High frequency content in nonlinear soil response: A numerical artifact or a reality?",* Soil Dynamics and Earthquake Engineering, 116:185–191, 2019.

[33] Weisstein, E. *"Fourier Series,"*
Available at ⟨http://mathworld.wolfram. com/FourierSeries.html⟩, accessed in January 2018.

[34] Xiaojun, Li. and Zheneng, Liao. *"Dynamic Skeleton Curve of Soil Stress Strain Relation under Irregular Cyclic Loading",* Earthquake Research in China, 7(4):469-477, 1993.

[35] Yu, G., Anderson, J.G., Siddarthan, R. *"On the characteristics of nonlinear soil response",* Bulletin of the Seismological Society of America, 83(1):218–244, 1992.

[36] Zeghal, M. et al. *"Lotung downhole array. II: evaluation of soil nonlinear properties,"* Journal of Geotechnical Engineering, 121(4):363–378, 1995.

[37] Zienkiewicz, O. C. et al. *"Static and DynamicBehaviour of Soils: A Rational Approach to Quantitative Solutions: I. Fully Saturated Problems"*, Proceedings of the Royal Society of London. A: Mathematical and Physical Sciences, A429(1877): 285-309, 1990.

APPENDIX

```
clear all
clc

%----------------Seed and Idriss (G/max and Damping ratio)--------------
G_Gmax=[1;  1;  0.99;   0.96;   0.85;   0.64;   0.37;   0.18;   0.08;   0.05;   0.035];

Am=[0.0001; 0.0003; 0.001;  0.003;  0.01;   0.03;   0.1;    0.3;    1;  3;  10]; %Amplitude of
shear strain for each cycle(in %)

dr=[0.0024; 0.0042; 0.008;  0.014;  0.028;  0.051;  0.098;  0.155;  0.21;   0.25;   0.28];

Gmax=811152.4096;  %shear modulus of soil

%shear modulus of soil
F=2;          %frequency of loading
T=1/F;
t=0:0.005:(1.25*T);    %time of loading sine wave (displacement)
w=2*3.14*F;
h=1;  %height of soil column
Am=Am*0.01;
L=length(Am);
g_ref=0.0088; %reference strain(Curve fit parameter (refer eq. (11))
A=1/Gmax;
B=1/g_ref/Gmax;
s=0.73;  (Curve fit parameter (refer eq. (11))
%tauy=Gmax*g_ref;  %For Cundall-Pyke rules
for j=1:L
   for i=1:length(t)
      u(i,j)=Am(j)*sin(2*3.14*F*t(i));    %displacement time history
   end
end

for j=1:L       %shear stress calculation (backbone curve nonlinear)
   Flag1=0;
      tau(1,j)=(u(i,j)/(A+(B*(abs(u(i,j)))^s)));
for i=2:length(t)
   du(i,j)=u(i,j)-u(i-1,j);
 if (u(i,j)-u(i-1,j)>=0 && Flag1==0)
      tau(i,j)=(u(i,j)/(A+(B*(abs(u(i,j)))^s)));
      D(i,j)=u(i,j);
      uns=u(i,j);
      Pun=tau(i,j);
 elseif(u(i,j)-u(i-1,j)<=0)
      Flag1=1;
      c=2;%abs(-1-(Pun/tauy));          %For Cundall-Pyke rules
      tau(i,j)=Pun+((u(i,j)-uns)/(A+B*(abs((u(i,j)-uns)/c))^s));
      D(i,j)=u(i,j);
      uns1=u(i,j);
```

```
        Pun1=tau(i,j);
    elseif (u(i,j)-u(i-1,j)>=0)
        c=2;%abs(1-(Pun1/tauy));          %For Cundall-Pyke rules
        tau(i,j)=Pun1+((u(i,j)-uns1)/(A+B*abs(abs((u(i,j)-uns1)/c))^s));
        D(i,j)=u(i,j);
        uns=u(i,j);
        Pun=tau(i,j);
    end
end
end

%-----------calculating unloading-reloading protion(excluding backbone curve)---------
for j=1:L
 for i=27:length(t)        %After 27 steps, the first unloading starts
     u1(i-26,j)=(D(i,j))/h;     %shear strain
     tau1(i-26,j)=tau(i,j);     %shear stress
 end
end

%-----------plotting unloading-reloading protion(excluding backbone curve)---------
    klp=1;
for j=1:1:L               %steps after which the loops are to be plotted
 for i=27:length(t)
     u1p(i-26,klp)=(D(i,j))/h;     %shear strain
     tau1p(i-26,klp)=tau(i,j);     %shear stress
 end
 klp=klp+1;
  plot(u1p,tau1p,'r')          %Hysteresis loops
 hold on;
end
grid on;
hold off;

%-----calculation and comparison of damping ratio and shear modulus------
for j=1:L
delW=0;
for i=1:(length(t)-26-1)
    delW=delW+(((tau1(i,j)+tau1(i+1,j))*0.5)*(u1(i+1,j)-u1(i,j)));
end
G(j)=(max(tau1(:,j)))/(max(u1(:,j)));
G_Gmaxd(j)=G(j)/Gmax;           %calculating G_Gmax from hysteresis loops
Ami(j)=(max(u1(:,j)));
W=(0.5*G(j)*max(u1(:,j))*max(u1(:,j)));
D_R(j)=(delW/W/4/3.14)+0.005014;     %with addition of small strain damping
end

figure(2);
semilogx(Ami,G_Gmaxd,'r');
hold on;
semilogx(Am,G_Gmax,'o--');
```

```
hold off;

figure (3);
semilogx(Am,dr,'b');
hold on;
semilogx(Ami,D_R,'o');
hold off;
```